# Evaluating the Time-Dependent Behavior of Deeply Buried Tunnels in Soft Rock environments and Relevant Measures Guaranteeing their Long-Term Stability

Wadslin Frenelus * and Hui Peng *

Posted Date: 6 September 2023

doi: 10.20944/preprints202309.0359.v1

Keywords: deeply buried tunnels; deep soft rocks; elasto-visco-plastic creep constitutive model; closed-form solutions; long-term stability; structural integrity; long-term monitoring

*Article*

# Evaluating the Time-Dependent Behavior of Deeply Buried Tunnels in Soft Rock environments and Relevant Measures Guaranteeing their Long-Term Stability

**Wadslin Frenelus * and Hui Peng ***

Department of Hydraulic Engineering, College of Hydraulic and Environmental Engineering, China Three Gorges University, Yichang, 443002, China; wadslin.frenelus@yahoo.com; wadslin@ctgu.edu.cn (WF); hpeng1976@163.com (H.P.)

* Correspondence: wadslin.frenelus@yahoo.com; wadslin@ctgu.edu.cn (WF); hpeng1976@163.com (H.P.)

**Abstract:** The time-dependent behavior and long-term stability of deep-buried tunnels in soft rocks have received lots of considerations in tunnel engineering and allied sciences. To better explore and deepen the engineering application of rock creep, extensive research studies are still needed, although fruitful outcomes have already obtained in many related investigations. In this article, the Weilai Tunnel in China's Guangxi province is studied taking its host rocks as the main research object. In fact, aiming at forecasting the time-varying deformation of this tunnel, a novel elasto-visco-plastic creep constitutive model with two variants is proposed, by exploiting the typical complex load-unload process of rock excavation. The model is well validated and good agreements are found with the relevant experimental data. Moreover, the time-dependent deformation rules are properly established for the surrounding rocks, by designing two new closed-form solutions based on the proposed creep model and the Hoek-Brown criterion. The convergence deformations calculated from the closed-form solutions conform well to the on-site monitoring data. In only 27 days after excavation, the creep deformation of the Weilai tunnel overtakes 400 mm, which is enormous. To guarantee the long-term stability of this tunnel, a robust support scheme and its long-term monitoring with appropriate remote sensors are strongly suggested.

**Keywords:** deeply buried tunnels; deep soft rocks; elasto-visco-plastic creep constitutive model; closed-form solutions; long-term stability; structural integrity; long-term monitoring

## 1. Introduction

Deep-buried tunnels are giant and costly engineering structures which are built all over the world owing to their multiple pertinent functions (mining, hydropower stations, transport, sanitary drainage systems, water supply, energy storage hosts, and so forth). Whatever the role of these underground structures, long-term safety and stability is usually strongly necessitated. Indeed, as time passes, the host rocks of deep tunnels tend to undergo displacements, and stability will be increasingly affected. The rock mass properties, the rigidity and the installation time of the support structure are among the major factors governing the displacements in the surrounding rocks of deep tunnels [1,2]. In fact, in deep rocky environments where there are durable actions of high stress, abundant groundwater, and fluctuated temperatures, the time-dependent deformation and long-term stability of the host rocks of deep underground tunnels are more and more concerned. This is due by the fact that gradual deformation of the surrounding rocks is inevitable once deeply buried tunnels are drilled. Owing to the unavoidable creep behavior of loaded rock materials [3,4], the development of microcracks around underground tunnels is imperative [5]. Creep is the time-dependent strength and deformations of rocks [6], and it is linked to the long-term stability of deep rock engineering. In the field of tunnel engineering, enormous progress and fruitful results have already been achieved. In spite of that, it is still difficult to guarantee the long-term stability of deep

Preprints (www.preprints.org) | NOT PEER-REVIEWED | Posted: 6 September 2023 doi:10.20944/preprints202309.0359.v1



soft rock tunnels which typically suffer from extreme rheology and are characterized by significant creep deformations. According to Zhu et al. [7], the consequences of dilatancy-induced high in-situ stress and the deformation caused by inadequate support are responsible for enormous deformation of such tunnels.

The time-dependent behavior and long-term stability of deep rock tunnels based on rock creep have been studied by many scholars and researchers. For example, Yang et al. [8] revealed that inordinate creep is the predominant cause of failure of deep underground storage structures. To combat the large deformation and ensure the stability of deep tunnels located in broken soft rock layers, Deng et al. [9] designed a creep model by taking the Burger Constitutive Viscoplastic (Burger model jointed to the Mohr-Coulomb body) model as a basis. They then analysed the possibility of optimizing the support scheme for these tunnels. A viscoelastic-plastic creep model was developed by Feng [10] to forecast time-dependent deformations of deep soft rock roadways mainly lodged in mudstone. For their part, Quevedo et al. [11] studied the long-term stability of deep tunnels using both the creep constitutive model of the surrounding rocks and that of the support, and emphasizing the long-lasting impact of creep on the support structure. Despite many abundant research results, in-depth studies on the long-term stability of deep soft rock tunnels are still needed. It should be highlighted that engineering situations vary from case to case. Ongoing research studies are thus required in order to continually improve and deepen the precise application of rock creep in tunnel engineering. Hence, the importance of this research study is considerable.

## 2. Study Area and Engineering Situation

The Weilai tunnel is located in Weilai Village, Bada Town, Xilin County, China's Guangxi Province. It is a component of the Tianxi Expressway project and belongs to the National Highway G357. The projected tunnel is a two-lane separation tunnel. The right line has a length of 662 m, and its starting and ending stakes are marked K114+422~K115+084. While the left line has a length of 686 m, and its starting and ending stakes are denoted Z4K114+424～Z4K115+110. In conformity with the engineering reports, the maximum burial depth of the tunnel is 105 m. Figure 1 provides a location map of the Weilai tunnel.

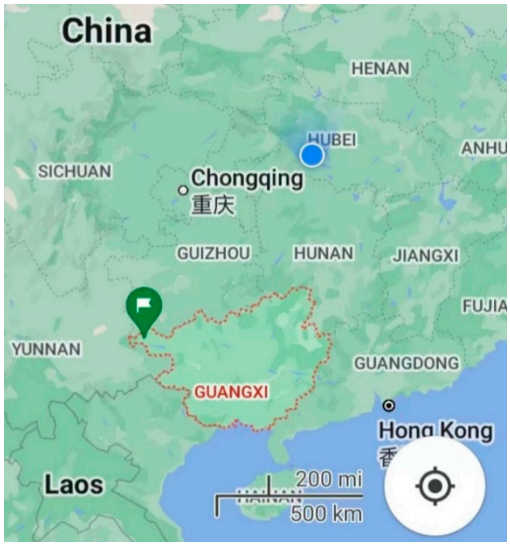


**Figure 1.** Location Map of the Weilai Tunnel.

### *2.1. Geology and Hydrology of the Tunnel Site*

The geological environment of the Weilai tunnel is complex. The tunnel site originates from the structural unit of the Xilin-Baise fault belt in the Youjiang regeneration trough of the Nanhua quasi-platform. Three evident structural developments (Caledonian, Indosinian-Yanshanian, and Himalayan) are encountered in the tunnel site. Besides, there are areas of large-scale sedimentary depressions. Huge mountains, intersecting ridges and valleys surround the tunnel site. Quaternary

Preprints (www.preprints.org) | NOT PEER-REVIEWED | Posted: 6 September 2023 doi:10.20944/preprints202309.0359.v1



residual slope accumulation characterizes the site and is mainly composed of argillaceous sandstone, sandstone, and mudstone. Nevertheless, argillaceous sandstone is the most predominant rock type in the tunnel alignment and is broken. The main lithology encountered along the tunnel route is schematized in Figure 2.

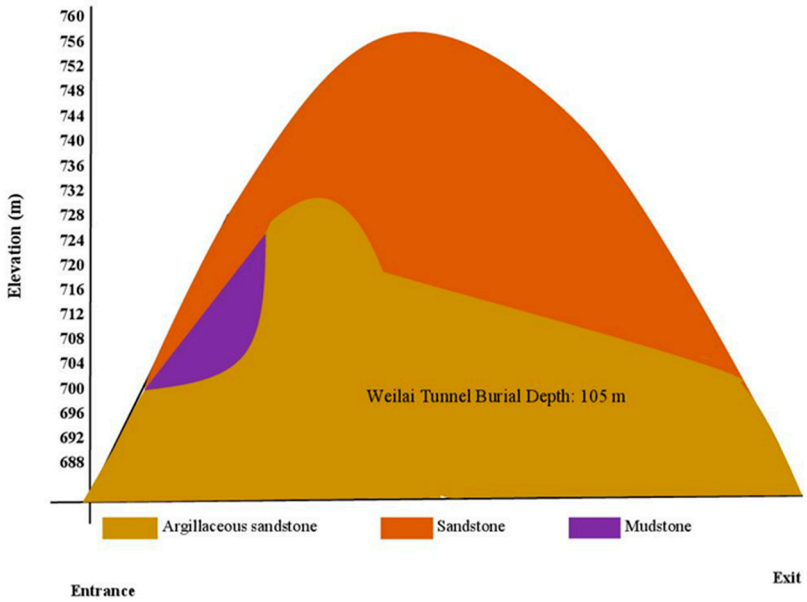


**Figure 2.** The main lithology along the tunnel route.

Groundwater inflows into the tunnel are mainly favored by the unfavorable geological conditions of the surrounding rocks and the availability of groundwater in the existing aquifers. In fact, it should be noted that karst terrains exist in a relatively large scale in Guangxi province which is located on the southeastern edge of the Yunnan-Guizhou Plateau. Typically, nearly 50% of groundwater inflows into rock tunnels are facilitated by karst terrains [12,13]. The risk level of tunnel construction in Guangxi is ordinarily increased by the ingress of groundwater into the host rocks.

*2.2. Excavation Method and Characteristics of the Surrounding Rocks*

Owing to the complexity of the tunnel site, drill-and-blast excavation method was imposed. Since the main rock type encountered in the tunnel alignment is broken and weakened, the blasting and the vibration velocity were scrupulously controlled. Throughout the entire line of the tunnel, based on a geological survey, the surroundings rocks are mainly categorized as class IV (soft rocks) and class V (broken soft rocks). Figure 3 illustrates the excavated tunnel subjected to a virgin in-situ stress $P_0$, and a view of the tunnel portal.

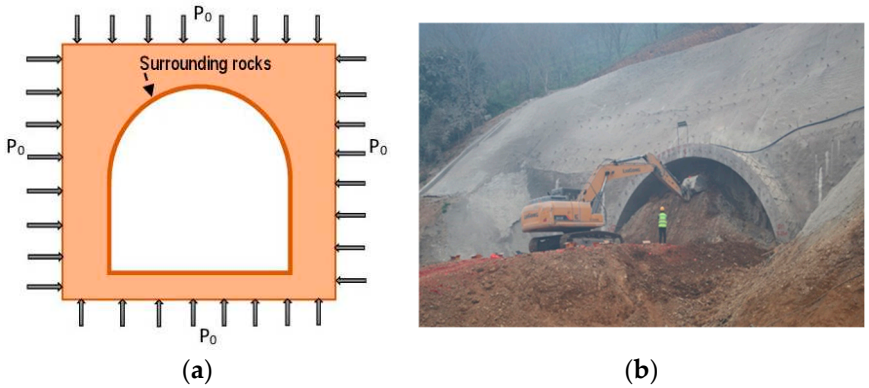


(**a**) (**b**)

**Figure 3.** Details of excavation: (**a**) excavated section; (**b**) a view of the tunnel portal.

Preprints (www.preprints.org) | NOT PEER-REVIEWED | Posted: 6 September 2023 doi:10.20944/preprints202309.0359.v1



Any excavation method provokes increased damage to the surrounding rocks of deep-buried tunnels. Nevertheless, drill-and-blast excavation has the reputation for causing significant damage to the rocks hosting the tunnels [14]. In fact, such excavation method is typically characterized by large unloading rate and short unloading time [15–17], and therefore considerably affects the relevant properties of the host rocks. More attentions should be paid to guarantee the long-term stability of deep-buried tunnels excavated by drill-and-blast method.

Based on relevant research outcomes [9,18–20], the average basic values of the physical-mechanical parameters of the host rocks are presented in Table 1 in dry states.

**Table 1.** Adopted average basic values for some rock parameters in dry states.

| Rock type | Uniaxial compressive strength (MPa) | Hydraulic Conductivity (m/s) | Elastic Modulus (GPa) | Poisson's ratio | Cohesion (MPa) | Internal friction angle (°) | Density ($g/cm^3$) |
|---|---|---|---|---|---|---|---|
| **Argillaceous sandstone** | 10 | | 2.2 | 0.23 | 5.06 | 30 | 0.24 |
| **Sandstone** | > 30 | $10^{-7.5}$ | 6.15 | 0.38 | 12.7 | 25 | 2.47 |

It is important to relatethat the rock parameters are be affected by the presence of groundwater in the regional environment of the tunnel. As already explained, due to the hydrological conditions of the tunnel site, groundwater effects cannot be neglected. Indeed, most rock parameters are diminished due to the effects of water [21,22]. Under wet conditions, uniaxial compressive strength, elastic modulus, internal friction, cohesion are generally reduced; while density and Poisson's ratio can be enhanced [23]. For wet conditions, the average values adopted for the physical-mechanical parameters of the host rocks are presented in Table 2.

**Table 2.** Adopted average values for some rock parameters in wet states.

| Rock type | Uniaxial compressive strength (MPa) | Hydraulic Conductivity (m/s) | Elastic Modulus (GPa) | Poisson's ratio | Cohesion (MPa) | Internal friction angle (°) | Density ($g/cm^3$) |
|---|---|---|---|---|---|---|---|
| **Argillaceous sandstone** | 6.6 | | 0.62 | 0.39 | 0.93 | 7.5 | 0.38 |
| **Sandstone** | >20 | $2 \times 10^{-7.5}$ | 1.74 | 0.60 | 2.31 | 6.25 | 3.95 |

## 3. Novel Creep Constitutive Model for the Host Rocks of the Weilai Tunnel

Conceiving the most appropriate constitutive relationship, able to correctly reflect the comportment of the host rocks, is a major task for addressing the long-term stability of deeply buried tunnels. To this end, mechanical models which are based on rheological approach, are largely utilized. Basically, springs, dashpots and frictional-cohesive elements are constituents of a given mechanical model [4,24,25]. A novel visco-elastic-plastic creep model that can be well exploited to study the long-term stability of the Weilai tunnel is of primary consideration. In fact, elasticity, plasticity, viscoelasticity and viscoplasticity coexist around the rheological deformation of rocks [26]. It is of tremendous importance to take into consideration such rock features in the design of a novel creep constitutive.

### *3.1. Adopted Creep Tests Data of Sandstone*

Adequate typical experimental data from triaxial creep tests under loading-unloading cycles for standard sandstone samples are utilized. Carried out by Yang et al. [27], the mentioned creep tests on deep sandstones reflect the conditions of the environment of the studied tunnel. Confining pressures (4 MPa, 8 MPa, and 12 MPa) were applied on the specimens which are subjected to load-unload cycles. Table 3 displays the different stress levels adopted for the deviatoric stress during the aforesaid tests.

Preprints (www.preprints.org) | NOT PEER-REVIEWED | Posted: 6 September 2023 doi:10.20944/preprints202309.0359.v1



**Table 3.** Load-unload schemes adopted for sandstone samples.

| Rock type | Confining pressure (MPa) | Deviatoric stress levels (MPa) | | | | |
|---|---|---|---|---|---|---|
| | | Level 1 | Level 2 | Level 3 | Level 4 | Level 5 |
| Sandstone | 4 | 11.99 | 14.99 | 17.99 | 20.97 | 23.98 |

Note that four traditional creep stage are generally manifested in soft rocks: instant elastic creep, primary creep, steady creep, and tertiary creep phases [25]. Figure 4 illustrates the staged load-unload of sandstone samples under a confining pressure of 4 MPa. Room temperature (25℃) was considered during the experiments.

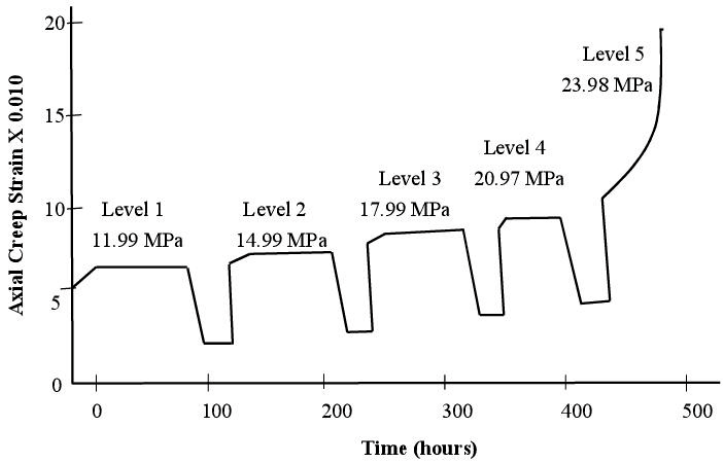


**Figure 4.** Staged load-unload of sandstone samples under a confining pressure of 4 MPa.

*3.2. Governing Equations and Proposed Mechanical Model*

It is widely recognized that tunnelling can be characterized by a complex cyclic load-unload [28–30]. Rock creep is therefore manifested in both loading and unloading stages, as illustrated in Figure 5. In such situation, the total creep strain can be written as below:

$$\varepsilon = \varepsilon_m + \varepsilon_v = \varepsilon_{me} + \varepsilon_{mp} + \varepsilon_{ve} + \varepsilon_{vp} \quad (1)$$

Here $\varepsilon$ stands for the total creep strain; $\varepsilon_m$ denotes the instant strain; $\varepsilon_v$ represents the creep strain; $\varepsilon_{me}$ is the instantaneous elastic strain; $\varepsilon_{mp}$ denotes the instant plastic strain; $\varepsilon_{ve}$ is the visco-elastic strain; $\varepsilon_{vp}$ represents the visco-plastic strain.

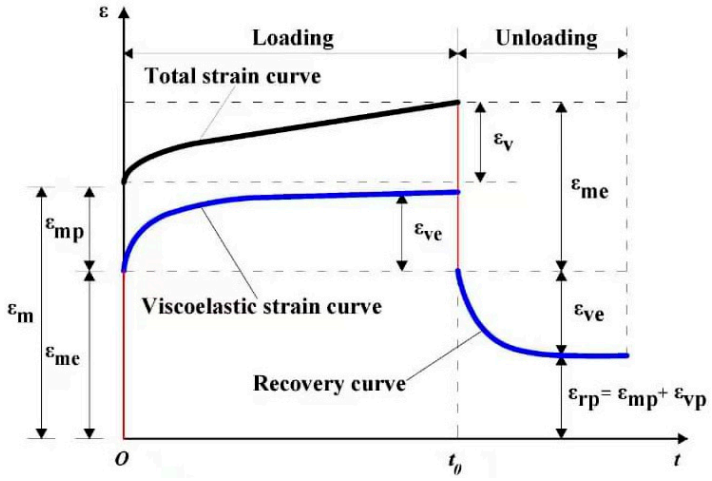


**Figure 5.** Creep curve of rocks subject to cyclic load-unload.

Preprints (www.preprints.org) | NOT PEER-REVIEWED | Posted: 6 September 2023 doi:10.20944/preprints202309.0359.v1



As previously mentioned, exploiting the complex load-unload process during tunnelling, and the coexistence of elasticity, plasticity, viscoelasticity and viscoplasticity in rock rheological deformation, the mechanical diagram of the proposed model is shown in Figure 6.

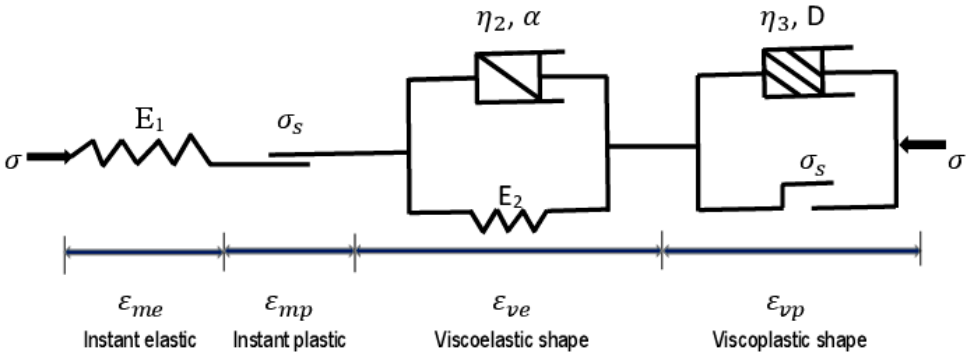


**Figure 6.** Mechanical diagram of the proposed visco-elasto-plastic creep model.

As shown in Figure 6, Hooke element, St. Venant, non-linear Kelvin, and visco-plastic element are the four components of the proposed creep model. This novel model has a great interest in capturing the creep behavior of the surrounding rocks of the Weilai tunnel. It constitutes the first variant of the model where dry states is considered.

*3.3. Development of the Proposed Creep Constitutive Model*

To simulate the instant elastic strain, the Hooke element is taken into account. Thereby, the axial instantaneous elastic strain can be read as follows [29,31]:

$$\varepsilon_{me} = \frac{\sigma}{E_1} \tag{2}$$

Here the applied stress is represented by $\sigma$, and the elastic modulus by $E_1$.

Regarding the axial instant plastic strain, referring to Sterpi and Gioda [32], it can be formulated by considering the modulus of the plastic deformation of the St. Venant element, $E_p$, and the scalar function, $I(\sigma_1 - \sigma_3 - \sigma_s)$, as follows:

$$\varepsilon_{mp} = \frac{\sigma - \sigma_s}{E_p} I(\sigma - \sigma_s) \tag{3}$$

The scalar function is defined as below:

$$I(\sigma - \sigma_s) = \begin{cases} 0, & \sigma < \sigma_s \\ 1, & \sigma \geq \sigma_s \end{cases} \tag{4}$$

Here $\sigma_s$ represents the long-term strength of rocks. Note that the long-term strength of rocks is of particular importance. In fact, due to aging and fatigue, rock strength diminishes with the passage of time [33]. In general, the instant rock strength is typically greater than the long-term strength. For soft rocks, the long-term strength is nearly ranged from 70%-80% of the instant value [33,34].

Concerning the visco-elastic element, it can be simulated by the non-linear Kelvin shape [35]. Assuming a constant $\alpha$ (material constant) can well reflect the inevitable influence of the stress level on rock creep, the nonlinear variant of the Kelvin model can be written in its differential constitutive equations as follows:

$$\sigma = E_2 \varepsilon_{ve} + \eta_2 t^{(1-\alpha)} \dot{\varepsilon}_{ve} \tag{5}$$

Here $\sigma$ is the applied stress, $E_2$ stands for the elastic modulus of the Kelvin shape, $\eta_2$ represents viscous coefficient of the Kelvin shape, $t$ is the creep time. The integration of the previous equation can lead to the following:

$$\varepsilon_{ve} = \frac{\sigma}{E_2}\left[1 - \exp\left(-\frac{E_2}{\eta_2 \alpha} t^{\alpha}\right)\right] \tag{6}$$

Preprints (www.preprints.org) | NOT PEER-REVIEWED | Posted: 6 September 2023 doi:10.20944/preprints202309.0359.v1



For the viscoplastic body, it can be described by improving the Ramberg-Osgood equation. Indeed, to improve the Ramberg-Osgood equation [36], in particular its plastic component, one considers the basic definition of rock creep where strain evolves with time, and under constant stress. Thereby, the visco-plastic creep strain model of soft rock can be written as follows:

$$\varepsilon_{vp} = k\sigma\left(\frac{t}{\eta_3(t)}\right)^n \tag{7}$$

Where $k$ and $n$ represent constant related to rock materials; $\sigma$ denotes the applied stress; $t$ is creep time; $\eta_3$ stands for coefficient of the initial viscosity of the viscoplastic body.

The variable damage ($D$) is introduced since it is of primary consideration at this stage. It should be noted that, under sustained effects of deviatoric stress, the evolution of damage in rock materials is unavoidable and one of the parameters which is affected by damage is the viscosity coefficient. Hence, the damaged viscosity coefficient can be expressed as below:

$$\eta_3(t) = \eta_3(1 - D) \tag{8}$$

Combining Equations (7) and (8), the visco-plastic creep strain can be expressed as follows:

$$\varepsilon_{vp} = k\sigma\left(\frac{t}{\eta_3}\right)^n (1 - D)^{(1-n)} \tag{9}$$

At the tertiary creep stage, as related by [37,38], the evolution of damage in rock materials can be widely expressed as follows:

$$\frac{D}{dt} = A\left(\frac{\sigma}{1-D}\right)^n \tag{10}$$

Here $A$ and $n$ are constants related to the materials. Under the evolution of time, critical or full scope of damage generally causes rock failure. Therefore, it is important to take into account the time-to-failure.

By solving the Equation (10) and by considering that $t = t_f$, where $t_f$ represents the rock time-to-failure, we can obtain the following:

$$\begin{cases} (1 - D)^{n+1} = 1 - A\sigma^n(1 + n)t \\ t_f = \frac{1}{A(1+n)\sigma^n} \end{cases} \tag{11}$$

Afterwards, the combination of equations (10) and (11) leads to the expression of the damage variable as below:

$$D = 1 - \left(1 - \frac{t}{t_f}\right)^{\frac{1}{1-n}} \tag{12}$$

Combining Equations (9) and (12), the visco-plastic creep strain can be expressed as follows:

$$\varepsilon_{vp} = k\sigma\left(\frac{t}{\eta_3}\right)^n \left(1 - \left[1 - \left(1 - \frac{t}{t_f}\right)^{\frac{1}{1-n}}\right]\right)^{(1-n)} \tag{13}$$

In its one dimension form, the novel creep model can be written as:

$$\varepsilon(t) = \frac{\sigma}{E_1} + \frac{\sigma}{E_2}\left[1 - exp\left(-\frac{E_2}{\eta_2\alpha}t^\alpha\right)\right] \qquad \sigma < \sigma_s \tag{14}$$

$$\varepsilon(t) = \frac{\sigma}{E_1} + \frac{\sigma-\sigma_s}{E_p} + \frac{\sigma}{E_2}\left[1 - exp\left(-\frac{E_2}{\eta_2\alpha}t^\alpha\right)\right] + k\sigma\left(\frac{t}{\eta_3}\right)^n \left(1 - \left[1 - \left(1 - \frac{t}{t_f}\right)^{\frac{1}{1-n}}\right]\right)^{(1-n)} \quad \sigma \geq \sigma_s \tag{15}$$

The three-dimensional form of the proposed creep model can be built by considering that rocks are typically in three-dimensional stress states. One assumes that creep is mainly provoked by the deviatoric stress tensor ($S_{ij}$), damage is accounted at the tertiary creep phase, and the Poisson's ratio of the rocks is not affected by time. The stress tensor ($\sigma_{ij}$) is mainly composed of the deviatoric stress tensor ($S_{ij}$) and the spherical tensor ($\sigma_m$).

Preprints (www.preprints.org) | NOT PEER-REVIEWED | Posted: 6 September 2023 doi:10.20944/preprints202309.0359.v1



On the basis of Hooke's law, the deviatoric stress tensor ($S_{ij}$) and the spherical stress tensor ($\sigma_m$) can be expressed as follows:

$$\begin{cases} S_{ij} = \sigma_{ij} - \varepsilon_m \delta_{ij} \\ \sigma_m = \frac{1}{3}(\sigma_1 + \sigma_2 + \sigma_3) \end{cases} \quad (16)$$

The shear or deviatoric strain tensor ($e_{ij}$), and the volumetric or spherical strain invariant ($\varepsilon_m$) are expressed as follows, where $\delta_{ij}$ stands for the Kronecker function:

$$\begin{cases} e_{ij} = \varepsilon_{ij} - \varepsilon_m \delta_{ij} \\ \varepsilon_m = \frac{1}{3}(\varepsilon_1 + \varepsilon_2 + \varepsilon_3) \end{cases} \quad (17)$$

The total strain ($\varepsilon_{ij}$) in three-dimensional form can be given by superimposing its components, by assuming that rocks are continuous media, as follows:

$$\varepsilon_{ij} = \varepsilon_{ij}^{me} + \varepsilon_{ij}^{mp} + \varepsilon_{ij}^{ve} + \varepsilon_{ij}^{vp} \quad (18)$$

Where $\varepsilon_{ij}^{me}$ and $\varepsilon_{ij}^{ve}$ represents respectively three-dimensional form of the instant elastic strain, and the visco-elastic strain; $\varepsilon_{ij}^{mp}$ and $\varepsilon_{ij}^{vp}$ are respectively three-dimensional form of the instant plastic strain, and visco-plastic strain.

The instant elastic strain ($\varepsilon_{ij}^{me}$) and the visco-elastic strain ($\varepsilon_{ij}^{ve}$) can be three-dimensionally expressed as follows:

$$\begin{cases} \varepsilon_{ij}^{me} = \frac{1}{2G_1} S_{ij} \\ \varepsilon_{ij}^{ve} = \varepsilon_{ij}^{ve} = \frac{1}{2G_2}\left[1 - exp\left(-\frac{G_2}{\eta_2 \alpha}\right) t^{\alpha}\right] S_{ij} \end{cases} \quad (19)$$

Here $G_1$ is shear modulus of elastic element; $S_{ij}$ represents the tensor of stress; $G_p$ is instant shear modulus; $S_s$ is the long-term strength of rock in three-dimensional form.

Likewise, the instant plastic strain ($\varepsilon_{ij}^{mp}$), and visco-plastic strain ($\varepsilon_{ij}^{vp}$) can be three-dimensionally written as follows:

$$\begin{cases} \varepsilon_{ij}^{mp} = \frac{S_{ij} - S_s}{G_p} \\ \varepsilon_{ij}^{vp} = \varepsilon_{ij}^{vp} = k S_{ij} \left(\frac{t}{\eta_3}\right)^n \left(1 - \left[1 - \left(1 - \frac{t}{t_f}\right)^{\frac{1}{1-n}}\right]\right)^{(1-n)} \end{cases} \quad (20)$$

The three-dimensional form of the proposed model can thus be read as below:

$$\varepsilon_{ij} = \begin{cases} \frac{1}{2G_1} S_{ij} + \frac{1}{2G_2}\left[1 - exp\left(-\frac{G_2}{\eta_2 \alpha} t^{\alpha}\right)\right] S_{ij} & (S_{ij} < S_s) \\ \frac{1}{2G_1} S_{ij} + \frac{S_{ij} - S_s}{G_p} + \frac{1}{2G_2}\left[1 - exp\left(-\frac{G_2}{\eta_2 \alpha} t^{\alpha}\right)\right] S_{ij} + k S_{ij} \left(\frac{t}{\eta_3}\right)^n \left(1 - \left[1 - \left(1 - \frac{t}{t_f}\right)^{\frac{1}{1-n}}\right]\right)^{(1-n)} & (S_{ij} \geq S_s) \end{cases} \quad (21)$$

With the variable damage D, the three-dimensional form of the proposed model can also be written as follows:

$$\varepsilon_{ij} = \begin{cases} \frac{1}{2G_1} S_{ij} + \frac{1}{2G_2}\left[1 - exp\left(-\frac{G_2}{\eta_2 \alpha} t^{\alpha}\right)\right] S_{ij} & (S_{ij} < S_s) \\ \frac{1}{2G_1} S_{ij} + \frac{S_{ij} - S_s}{G_p} + \frac{1}{2G_2}\left[1 - exp\left(-\frac{G_2}{\eta_2 \alpha} t^{\alpha}\right)\right] S_{ij} + k S_{ij} \left(\frac{t}{\eta_3}\right)^n (1 - D)^{(1-n)} & (S_{ij} \geq S_s) \end{cases} \quad (22)$$

The axial stress deviator ($S_{11}$), for the maximum stress direction, is given by:

$$S_{11} = \sigma_1 - \sigma_m = \frac{2}{3}(\sigma_1 - \sigma_3) \quad (23)$$

Thereby, in the maximum stress direction, the creep model can be computed as:

$$\varepsilon_{11}(t) = \begin{cases} \frac{\sigma_1 - \sigma_3}{3G_1} + \frac{\sigma_1 - \sigma_3}{3G_2}\left(1 - exp\left(-\frac{G_2}{\eta_2 \alpha} t^{\alpha}\right)\right) & (S_{ij} < S_s) \\ \frac{\sigma_1 - \sigma_3}{3G_1} + \frac{2(\sigma_1 - \sigma_3) - 3\sigma_s}{3G_p} + \frac{\sigma_1 - \sigma_3}{3G_2}\left(1 - exp\left(-\frac{G_2}{\eta_2 \alpha} t^{\alpha}\right)\right) + \frac{2k}{3}(\sigma_1 - \sigma_3)\left(\frac{t}{\eta_3}\right)^n \left(1 - \left[1 - \left(1 - \frac{t}{t_f}\right)^{\frac{1}{1-n}}\right]\right)^{(1-n)} & (S_{ij} \geq S_s) \end{cases} \quad (24)$$

Preprints (www.preprints.org) | NOT PEER-REVIEWED | Posted: 6 September 2023 doi:10.20944/preprints202309.0359.v1



The unloading of the applied stress is assumed to be happened at time $t_0$. As such, the three-dimensional form of the proposed creep model can be converted into the following unloading equations:

$$\varepsilon_{11}(t) = \frac{\sigma_1-\sigma_3}{3G_2}\left(1 - exp\left(-\frac{G_2}{\eta_2\alpha}t_0^{\alpha}\right)\right)exp\left(\frac{G_2}{\eta_2 t_0^{1-\alpha}}(t_0 - t)\right) \quad (25)$$

3.3.1. Identification of Model Parameters

Designed to depict the creep behavior of soft rocks, the novel creep model takes into account several parameters such as elastic, plastic and viscous. The shear modulus $G_1$ can be assessed as below:

$$G_1 = \frac{E}{2(1+\nu)} \quad (26)$$

Where $\nu$ denotes poisson's ratio; and E elastic modulus.

To evaluate $G_p$, the experimental data related to instant plastic creep strains are employed. Concerning the determination of $G_2$ and $\alpha$, Equation (32) is used. Note that, under the conditions of the time $t$ is infinitely large, and $\sigma < \sigma_s$, the aforesaid equations can be modified as follows:

$$\varepsilon = \frac{\sigma_1-\sigma_3}{3G_1} + \frac{\sigma_1-\sigma_3}{3G_2} \quad (27)$$

Besides, under the aforementioned conditions, adequate operations are utilized. The subtraction of equation (24) into equation (27) provides the following:

$$\text{Equation (24)} - \text{Equation (27)} = \left(\frac{\sigma_1-\sigma_3}{3G_2}\right)exp\left(-\frac{G_2}{\eta_2\alpha}t^{\alpha}\right) \quad (28)$$

Also, when $\sigma < \sigma_s$ and $t \to \infty$, we can get:

$$ln\ (\text{Equation (27)} - \text{Equation (24)}) = \ln\left[\frac{\sigma_1-\sigma_3}{3G_2}exp\left(-\frac{G_2}{\eta_2\alpha}t^{\alpha}\right)\right] = ln\left(\frac{\sigma_1-\sigma_3}{3G_2}\right) - \frac{G_2}{\eta_2\alpha}t^{\alpha} \quad (29)$$

Equation (29) is a function in which $t$ is the variable. It can be formulated as below:

$$f(t) = ln\left(\frac{\sigma_1-\sigma_3}{3G_2}\right) - \frac{G_2}{\eta_2\alpha}t^{\alpha} \quad (30)$$

A nonlinear function can describe the previous function. The general form is as follows:

$$f(t) = q + mt^k \quad (31)$$

Here $m$, $k$, and $q$ are fitting parameters.

By identifying common terms in the equations (30) and (31), we can get:

$$\begin{cases} m = -\frac{G_2}{\eta_2\alpha} \\ \alpha = k \\ q = ln\left(\frac{\sigma_1-\sigma_3}{3G_2}\right) \end{cases} \quad (32)$$

The fitting parameters can be used to evaluate $G_2$, $\eta_2$, and $\alpha$. As such, $G_2$, $\eta_2$, and $\alpha$ can be found to be:

$$\begin{cases} G_2 = \frac{\sigma_1-\sigma_3}{3e^q} \\ \alpha = k \\ \eta_2 = \frac{\sigma_1-\sigma_3}{3mke^q} \end{cases} \quad (33)$$

The nonlinear least square method of Levenberg–Marquardt [39] is utilized to determine the viscosity coefficients $\eta_2$ and $\eta_3$, and the constant of rock materials $n$,. For the fitting of creep test data, a typical parametric equation can be employed as below:

$$\varepsilon = A' + B' + C'\left(1 - e^{-D't}\right) + E'\left[1 - \left(1 - \frac{t}{t_f}\right)^{F'}\right]^{G'} \quad (34)$$

Preprints (www.preprints.org) | NOT PEER-REVIEWED | Posted: 6 September 2023 doi:10.20944/preprints202309.0359.v1



Here $\varepsilon$ stands for the total creep strain of the designed model; the fitting parameters are $A', B', C', D', E'$, and $F'$ which are written as follows:

$$\begin{cases} A' = \frac{\sigma_1-\sigma_3}{3G_1} \\ B' = \frac{2(\sigma_1-\sigma_3)-3\sigma_s}{3G_p} \\ C' = \frac{\sigma_1-\sigma_3}{3G_2} \\ D' = \frac{G_2}{\eta_2\alpha} \\ E' = \frac{2k}{3}(\sigma_1-\sigma_3)\left(\frac{t}{\eta_3}\right)^n \\ F' = \frac{1}{1-n} \\ G' = 1-n \end{cases} \tag{35}$$

Equations (34) and (35) can be combined as follows:

$$\varepsilon_{11}(t) = \begin{cases} A' + C'\left(1-exp(-D't^{\alpha})\right) & (\sigma < \sigma_s) \\ A' + B' + C'\left(1-exp\left(-D't^{\alpha}\right)\right) + E'\left[1-\left(1-\frac{t}{t_f}\right)^{F'}\right]^{G'} & (\sigma \geq \sigma_s) \end{cases} \tag{36}$$

3.3.2. Validation of the Proposed Model

The model is verified in good agreement with the results of creep tests under triaxial cyclic load-unload cycles. The coefficient of determination ($R^2$) is employed to check the model accuracy. Broadly speaking, the peak value of $R^2$ is 1. Higher values of $R^2$ correspond to higher accuracies. The coefficient of determination ($R^2$) is expressed as:

$$R^2 = 1 - \frac{\sum_{i=1}^{n}(y_c-y_i)^2}{\sum_{i=1}^{n}(y_c-\overline{y_i})^2} \tag{37}$$

Here $n$ represents the amount of test data points; $y_c$ stands for calculated values; $y_i$, and $\overline{y_i}$ denotes respectively the test value and its average.

In Tables 4 and 5, respectively for loading and unloading conditions, the calculated parameters of the model are presented.

**Table 4.** Parameters of the model at diverse stress levels in loading states.

| $\sigma_1-\sigma_3$ (MPa) | $G_1$ (GPa) | $G_p$ (GPa) | $G_2$ (GPa) | $\eta_2$ (GPa.$h$) | $\eta_3$ (GPa.h) | $\alpha$ | $n$ | $k$ | $t_f$ (h) | $R^2$ |
|---|---|---|---|---|---|---|---|---|---|---|
| 11.99 | 2.23 | 3.14 | 4.39 | 19.25 | | 1.152 | | | | 0.9835 |
| 14.99 | 1.92 | 8.73 | 5.59 | 38.97 | | 0.091 | | | | 0.9914 |
| 17.99 | 1.61 | 8.98 | 9.16 | 509.88 | | 0.023 | | | | 0.9921 |
| 20.97 | 1.69 | 21.14 | 13.25 | 104.77 | | 0.762 | | | | 0.9875 |
| 23.98 | 1.72 | 0.68 | 6.11 | 558.23 | 0.897 | 0.811 | 12.01 | 0.02 | 585 | 0.9946 |

Preprints (www.preprints.org) | NOT PEER-REVIEWED | Posted: 6 September 2023 doi:10.20944/preprints202309.0359.v1



**Table 5.** Parameters of the model at diverse stress levels in unloading states.

| $\sigma_1 - \sigma_3$ (MPa) | $G_p$ (GPa) | $G_2$ (GPa) | $\eta_2$ (GPa.$h$) | $\alpha$ | $R^2$ |
|---|---|---|---|---|---|
| 11.99 | 2.72 | 0.023 | 0.0364 | 1.51 | 0.9835 |
| 14.99 | 4.94 | 0.12 | 0.0085 | 26.02 | 0.9932 |
| 17.99 | 10.11 | 0.49 | 0.0213 | 25.07 | 0.9854 |
| 20.97 | 3.45 | 0.25 | 0.0158 | 11.73 | 0.9897 |

In order to ensure proper validation, comparisons are made between creep strains calculated from the model and the pertinent experimental data. Under different levels of the deviatoric stress, the results are displayed in Figures 7 to 11.

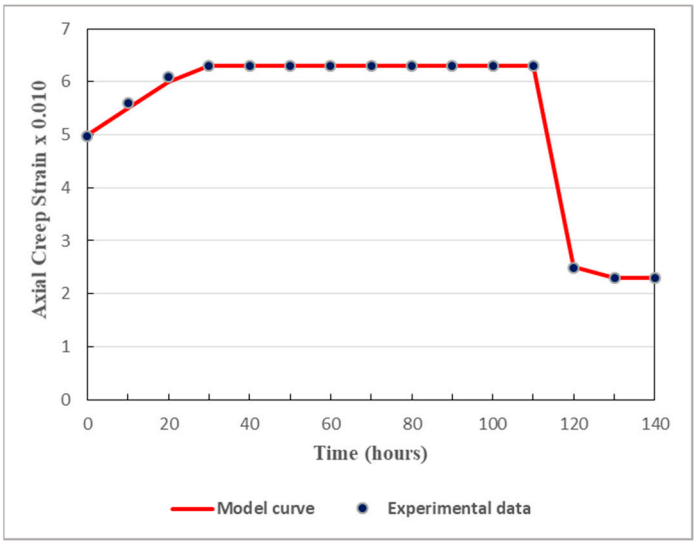


**Figure 7.** Model curve compared to experimental data for sandstone under a deviatoric stress of 11.99 MPa.

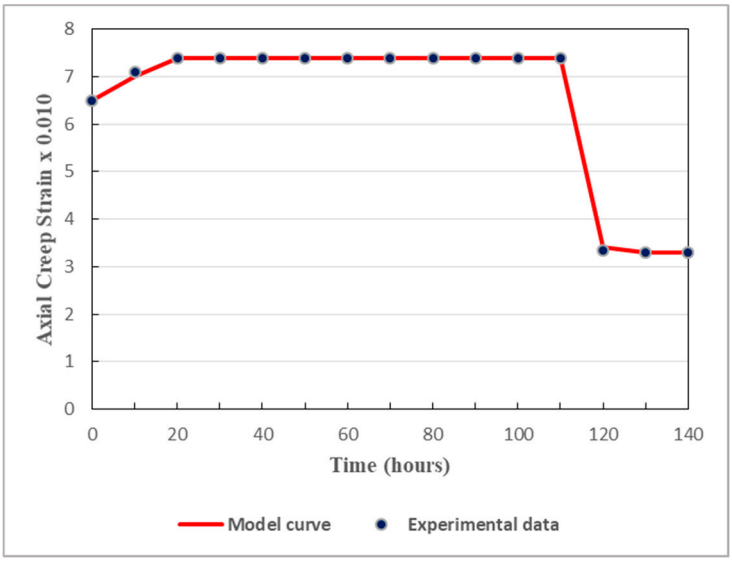


**Figure 8.** Model curve compared to experimental data for sandstone under a deviatoric stress of 14.99 MPa.

Preprints (www.preprints.org) | NOT PEER-REVIEWED | Posted: 6 September 2023 doi:10.20944/preprints202309.0359.v1



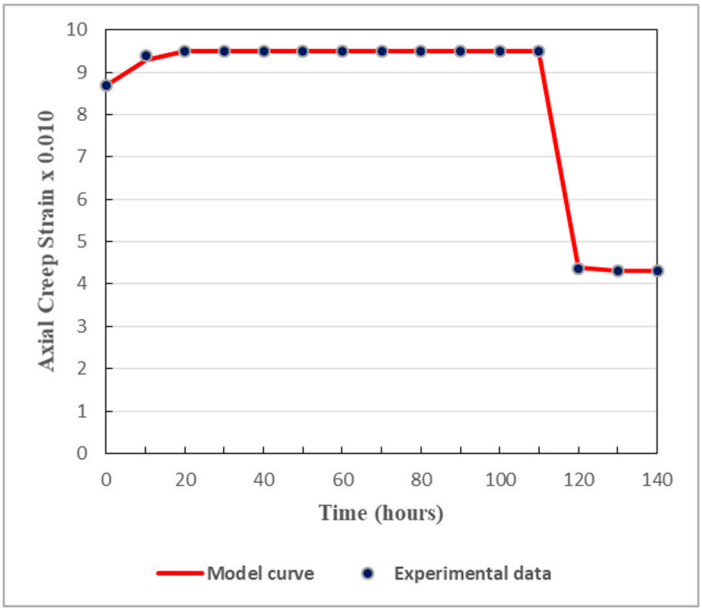


**Figure 9.** Model curve compared to experimental data for sandstone under a deviatoric stress of 17.99 MPa.

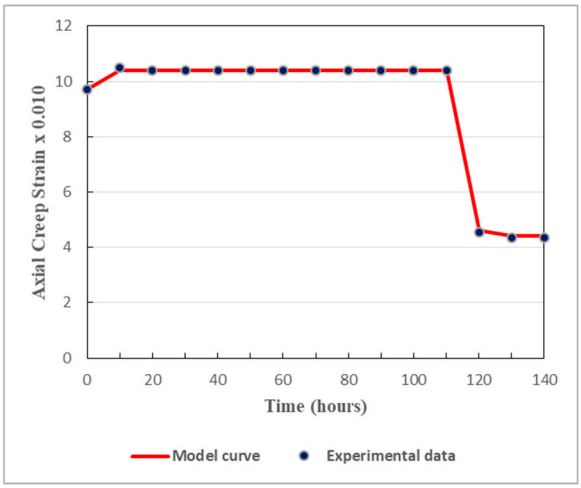


**Figure 10.** Model curve compared to experimental data for sandstone under a deviatoric stress of 20.97 MPa.

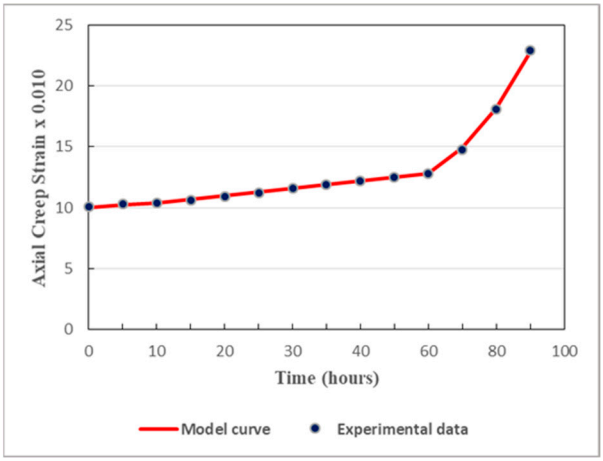


**Figure 11.** Model curve compared to experimental data for sandstone under a deviatoric stress of 23.98 MPa.

Preprints (www.preprints.org) | NOT PEER-REVIEWED | Posted: 6 September 2023 doi:10.20944/preprints202309.0359.v1



As displayed in Figures 7 to 11, both in the loading stage and in the unloading stage, the model is in good agreement with the experimental data. The proposed model can thus well simulate the creep behavior of the studied tunnel. It can be remarked that there is huge difference between the values obtained from the loading stage and those obtained from the unloading stage. In fact, the unloading process has considerable effects on the mechanical properties of soft rocks. Since cracks generally tend to evolve rapidly in unloaded rocks, the rock relevant mechanical properties are affected by the unloading phase and then altered to some extent. It should be noted that, generally, soft rocks have lesser abilities to withstand deformations generated by the unloading stage than those caused by the loading stage. This is why rock rupture can be faster during the unloading process than during the loading process. Thereby, when studying the long-term safety and stability of deeply buried tunnels, the cyclic loading-unloading process of the host rocks plays a key role.

There is rapid evolution of the creep process of sandstone, under the deviatoric stress of 23.98 MPa, as revealed in Figure 11. As the stress level is high, there is rapid appearance of the tertiary creep. In fact, high deviatoric stress is capable of shortening the duration of steady creep and hastening the triggering of the tertiary creep. At a high stress level, the rapid onset of the tertiary will seriously jeopardize the long-term stability of the tunnel. Appropriate measures are quickly needed to ensure the longest duration of steady creep in deep rock tunnels subject to high geostresses.

### 3.3.3. Effect of Pore Water Pressure: Second Variant of the Proposed Model

The influence of pore water pressure cannot be overlooked since the predominant rock type of the studied tunnel is broken, and groundwater is abundant in the concerned media. Seepage actions can be severe in this rocky environment. They can generally reduce the bearing capacity of the support structure by modifying the stress allotments around the overall tunnel components [40]. Thereby, it is of tremendous consideration to take into account the influence of pore water pressure on the creep process. To this end, damage is particularly accounted in the tertiary creep. It is well known that damage augments as tertiary creep stage evolves. Therefore, in order to account the effects of pore water pressure on rock creep, the damage variable is employed. In this situation, the damage variable can be read as below, where $\beta\ (\sigma, p)$ is a material constant which is affected by pore water pressure ($p$) and stress ($\sigma$):

$$D = 1 - e^{-\beta\ (\sigma,\ p)t} \tag{38}$$

A variant of the mechanical model which is affected by pore water pressure is presented in Figure 12.

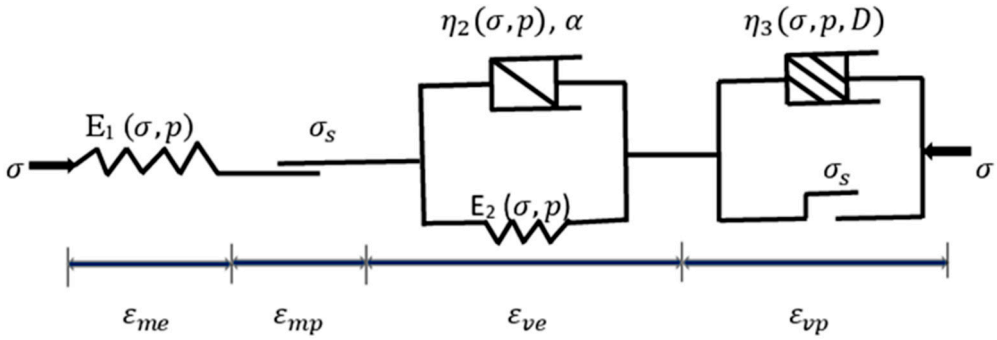


**Figure 12.** Mechanical model influenced by pore water pressure.

Jointed influence of pore water pressure and confining pressure is taken into account. This influence can be written, for the visco-plastic element, as follows:

$$\eta_3(\ \sigma\ , p, D) = \eta_3(\ \sigma\ , p)(1 - D) \tag{39}$$

Equations (22), (38), and (39) are adequately combined. The three-dimensional form of the novel creep model with effects of pore water pressure can be written as:

Preprints (www.preprints.org) | NOT PEER-REVIEWED | Posted: 6 September 2023 doi:10.20944/preprints202309.0359.v1



$$\varepsilon_{ij}(t,\sigma,p)=\begin{cases}\frac{1}{2G_1(\sigma,p)}S_{ij}+\frac{1}{2G_2(\sigma,p)}\left[1-exp\left(-\frac{G_2(\sigma,p)}{\eta_2(\sigma,p)\alpha}t^{\alpha}\right)\right]S_{ij} & (S_{ij}<S_s)\\ \frac{1}{2G_1(\sigma,p)}S_{ij}+\frac{S_{ij}-S_s}{G_p(\sigma,p)}+\frac{1}{2G_2(\sigma,p)}\left[1-exp\left(-\frac{G_2(\sigma,p)}{\eta_2(\sigma,p)\alpha}t^{\alpha}\right)\right]S_{ij}+kS_{ij}\left(\frac{t}{\eta_3(\sigma,p)}\right)^n\left(e^{-\beta(\sigma,\ p)t}\right)^{(1-n)} & (S_{ij}\geq S_s)\end{cases} \quad (40)$$

Also, for the maximum stress direction, the model affected by pore pressure can be read as follows:

$$\varepsilon_{11}(t,\sigma,p)=\begin{cases}\frac{\sigma_1-\sigma_3}{3G_1(\sigma,p)}+\frac{\sigma_1-\sigma_3}{3G_2(\sigma,p)}\left(1-exp\left(-\frac{G_2(\sigma,p)}{\eta_2(\sigma,p)\alpha}t^{\alpha}\right)\right) & (\sigma<\sigma_s)\\ \frac{\sigma_1-\sigma_3}{3G_1(\sigma,p)}+\frac{2(\sigma_1-\sigma_3)-3\sigma_s}{3G_p(\sigma,\ p)}+\frac{\sigma_1-\sigma_3}{3G_2(\sigma,p)}\left(1-exp\left(-\frac{G_2(\sigma,p)}{\eta_2(\sigma,p)\alpha}t^{\alpha}\right)\right)+\frac{2k}{3}(\sigma_1-\sigma_3)\left(\frac{t}{\eta_3(\sigma,p)}\right)^n\left(e^{-\beta(\sigma,\ p)t}\right)^{(1-n)} & (\sigma\geq\sigma_s)\end{cases} \quad (41)$$

Taking into consideration the variation trend in the mechanical properties of the soft rocks subjected to pore water pressure change [41], the parameters of the model are scrupulously evaluated for three levels (0.05 MPa, 0.10 MPa, 0.15 MPa) of pore water pressure. Tables 6 and 7 show the parameters.

**Table 6.** Model parameters affected by pore water pressure ($p$) in the loading states.

| $p$ (MPa) | $\sigma_1-\sigma_3$ (MPa) | $G_1$ (GPa) | $G_p$ (GPa) | $G_2$ (GPa) | $\eta_2$ (GPa.$h$) | $\eta_3$ (GPa.h) | $\alpha$ | $n$ | $k$ | $t_f$ (h) | $R^2$ |
|---|---|---|---|---|---|---|---|---|---|---|---|
| 0.05 | 11.99 | 2.67 | 3.76 | 5.26 | 15.41 | | 1.021 | | | | 0.9917 |
| | 14.99 | 2.30 | 10.47 | 6.70 | 31.17 | | 0.082 | | | | 0.9877 |
| | 17.99 | 1.93 | 10.77 | 10.99 | 407.90 | | 0.020 | | | | 0.9873 |
| | 20.97 | 2.02 | 25.36 | 15.90 | 83.81 | | 0.687 | | | | 0.9889 |
| | 23.98 | 5.16 | 0.81 | 7.33 | 446.58 | 0.69 | 0.782 | 11.64 | 0.024 | 552 | 0.9914 |
| 0.10 | 11.99 | 2.60 | 3.65 | 5.11 | 36.57 | | 0.975 | | | | 0.9921 |
| | 14.99 | 2.23 | 10.17 | 6.51 | 74.00 | | 0.077 | | | | 0.9981 |
| | 17.99 | 1.87 | 10.47 | 10.68 | 968.77 | | 0.018 | | | | 0.9823 |
| | 20.97 | 1.97 | 24.64 | 15.44 | 198.06 | | 0.754 | | | | 0.9789 |
| | 23.98 | 2.00 | 0.79 | 7.12 | 1060.63 | 1.65 | 0.783 | 9.72 | 0.035 | 489 | 0.9911 |
| 0.15 | 11.99 | 2.70 | 3.52 | 5.04 | 13.59 | | 0.942 | | | | 0.9918 |
| | 14.99 | 2.33 | 9.79 | 6.42 | 27.51 | | 0.075 | | | | 0.9845 |
| | 17.99 | 1.95 | 10.06 | 10.53 | 358.01 | | 0.018 | | | | 0.9872 |
| | 20.97 | 2.05 | 23.72 | 15.63 | 73.96 | | 0.741 | | | | 0.9886 |
| | 23.98 | 2.08 | 0.76 | 7.20 | 394.11 | 0.63 | 0.771 | 10.85 | 0.041 | 447 | 0.9929 |

**Table 7.** Model parameters affected by pore water pressure in the unloading states.

| $p$ (MPa) | $\sigma_1-\sigma_3$ (MPa) | $G_p$ (GPa) | $G_2$ (GPa) | $\eta_2$ (GPa.$h$) | $\alpha$ | $R^2$ |
|---|---|---|---|---|---|---|
| 0.05 | 11.99 | 2.01 | 0.014 | 0.0312 | 1.62 | 0.9911 |
| | 14.99 | 4.23 | 0.08 | 0.0071 | 27.87 | 0.9869 |
| | 17.99 | 9.34 | 0.28 | 0.0202 | 28.15 | 0.9881 |
| | 20.97 | 3.02 | 0.19 | 0.0112 | 12.63 | 0.9874 |
| 0.10 | 11.99 | 2.33 | 0.018 | 0.0605 | 1.73 | 0.9928 |
| | 14.99 | 4.23 | 0.105 | 0.0137 | 27.98 | 0.9891 |
| | 17.99 | 4.93 | 0.37 | 0.0392 | 28.43 | 0.9799 |
| | 20.97 | 3.50 | 0.25 | 0.0217 | 13.02 | 0.9898 |
| 0.15 | 11.99 | 2.76 | 0.020 | 0.0427 | 1.77 | 0.9976 |

Preprints (www.preprints.org) | NOT PEER-REVIEWED | Posted: 6 September 2023 doi:10.20944/preprints202309.0359.v1



| | | | | | | |
|---|---|---|---|---|---|---|
| | 14.99 | 4.35 | 0.119 | 0.0112 | 28.64 | 0.9854 |
| | 17.99 | 5.11 | 0.41 | 0.0264 | 29.58 | 0.9887 |
| | 20.97 | 3.67 | 0.28 | 0.0197 | 14.01 | 0.9985 |

Under loading and unloading conditions, Figures 13 to 15 present the effects of pore water pressure on the evolution of rock creep.

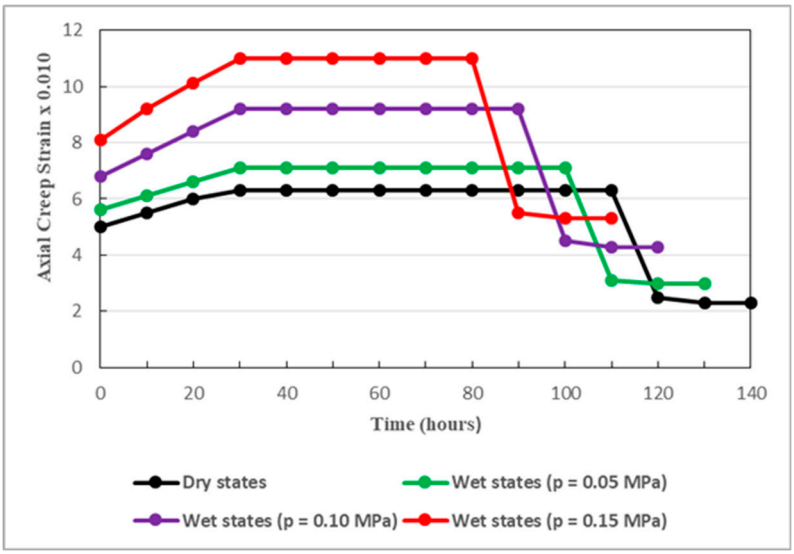


**Figure 13.** Creep strain of sandstone affected by pore water pressure (the deviatoric stress is 11.99 MPa).

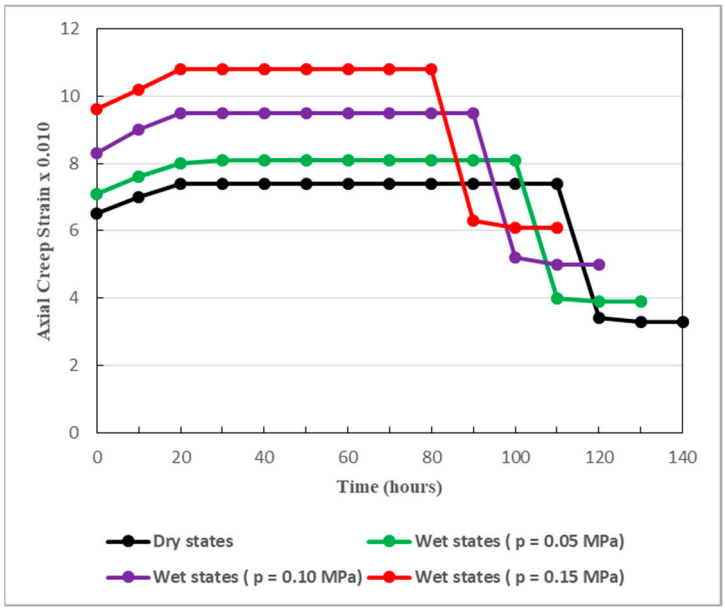


**Figure 14.** Creep strain of sandstone affected by pore water pressure (the deviatoric stress is 17.99 MPa).

Preprints (www.preprints.org) | NOT PEER-REVIEWED | Posted: 6 September 2023 doi:10.20944/preprints202309.0359.v1



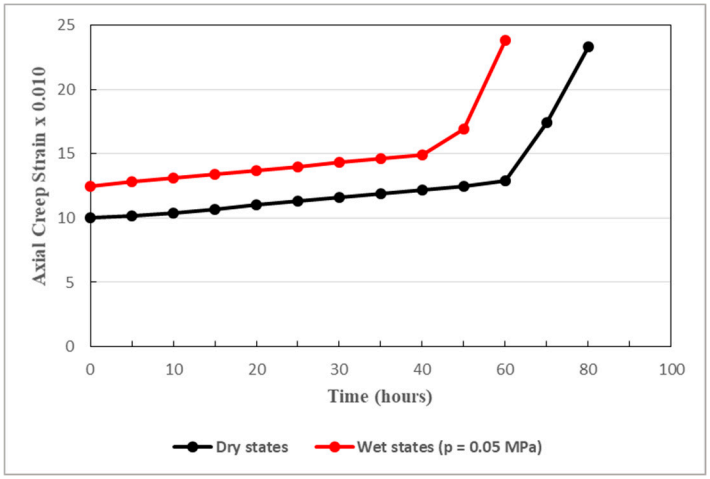


**Figure 15.** Creep strain of sandstone affected by pore water pressure (the deviatoric stress is 23.98 MPa).

Figures 13 to 15 clearly reveal that pore water pressure seriously affects the creep process of the rocks surrounding the studied tunnel. The creep strain increases and the creep life of the rock decreases when pore water pressure increases. In fact, the higher the pore pressure, the faster the creep process evolves. Pore water pressure shortens the duration of both loading and unloading processes. It is one of the major factors causing considerable instability in deep rock engineering. It can even provoke unexpected failure of deep soft rocks subjected to elevated stress, as it can be interpreted in Figure 15.

Figure 15 shows that, even under low pore water pressure, with the effects of pore water pressure, the creep of sandstone develops more rapid that than in dry conditions. Indeed, with the influence of pore water pressure, the tertiary creep triggers earlier after only 40 hours. However, in dry conditions, tertiary creep happens nearly after 60 hours. In the context of long-term stability of the deep soft rock tunnel, the effects of the pore water pressure must be strongly addressed.

## 4. Closed-Form Solutions and Convergence Deformation of the Weilai Tunne

Reliable closed-form solutions are necessary to assess the time-dependent deformation of deep-buried tunnels particularly built in complex rocky media. The proposed creep constitutive with its two variants has to be converted into two closed-form solutions. To do this, a suitable tunnel mechanical model is adopted. As shown in Figure 16, the tunnel is subjected to a virgin in situ stress field ($P_0$). It is assimilated to a circular tunnel where the radius is $R_0$. The rocks surrounding the tunnel deform elastically, viscoelastically, plastically and viscoplastically. The distance between the center of the tunnel and the limit of the viscoplastic zone is denoted by $R_P$. The actual cross section geometry has two parts which comprises a semi-circular part (the upper part), and a rectangular part (the lower part). For calculation and analysis convenience, and referring to Peng et al. [42], it is assumed that a circular section can represent the two sections.

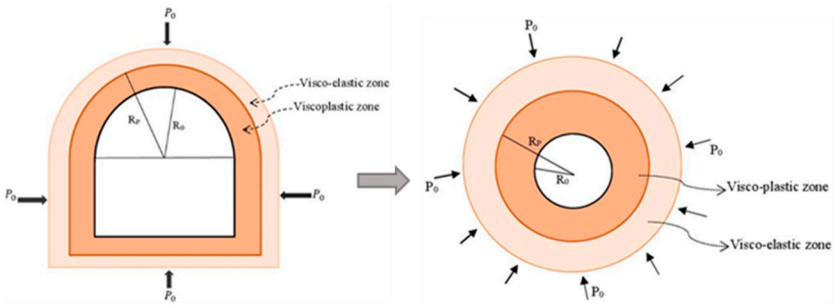


**Figure 16.** Adopted mechanical model of the studied tunnel.

Preprints (www.preprints.org) | NOT PEER-REVIEWED | Posted: 6 September 2023 doi:10.20944/preprints202309.0359.v1



In the post-excavation phase, the actual state of the tunnel can be described by two main zones namely, the internal and the external zones. The visco-plastic conditions are depicted by the internal zones; and the visco-elastic states by the external zones. Typically, the nonlinear failure characteristics of rocks can be described by the Hoek–Brown criterion where the concerned elastic and plastic parameters can be defined. Thereby, parameters in the elastic and plastic zones can be respectively given as follows [43–45]:

$$\begin{cases} \sigma_r^e = P_0 - \frac{R_0^2}{r^2} N_1 e^{2M} \\ \sigma_\theta^e = P_0 + \frac{R_0^2}{r^2} N_1 e^{2M} \\ \sigma_z^e = P_0 \\ M = \frac{\sqrt{m^2 + \frac{16mP_0}{\sigma_c} + 16s} - 4\sqrt{s} - m}{2m} \\ N_1 = P_0 - M\sigma_c\sqrt{s} - M^2 \frac{m\sigma_c}{4} \end{cases} \tag{42}$$

$$\begin{cases} \sigma_r^p = \frac{m\sigma_c}{4}\left(ln\frac{r}{R_0}\right)^2 + \sigma_c\sqrt{s}ln\left(\frac{r}{R_0}\right) \\ \sigma_\theta^p = \frac{m\sigma_c}{4}\left(ln\frac{r}{R_0}\right)^2 + (\frac{m\sigma_c}{2} + \sigma_c\sqrt{s})ln\left(\frac{r}{R_0}\right) + \sigma_c\sqrt{s} \\ \sigma_z^p = \frac{(1+\sin\theta)\sigma_\theta^p + (1-sin\theta)\sigma_r^p}{2} \\ R_P = R_0 e^M \end{cases} \tag{43}$$

Here the radial elastic stress, axial elastic stress, and hoop elastic stress, are respectively noted by $\sigma_r^e$, $\sigma_z^e$, $\sigma_\theta^e$. For intact rocks, the unconfined compressive strength is represented by $\sigma_c$. Likewise, the radial plastic stress, axial plastic stress, and hoop plastic stress, are respectively noted by $\sigma_r^p$, $\sigma_z^p$, $\sigma_\theta^p$. The distance related to the central point of the section of the tunnel is noted by $r$. The dilation angle is indicated by $\phi$, and is given by:

$$\phi = \frac{5GSI - 125}{1000}\varphi \tag{44}$$

Here $GSI$ is Geological Strength Index; $\varphi$ denotes internal friction angle of the rock. The material parameters are $m_b$ and $s$, and can be determined as follows:

$$\begin{cases} m_b = m_i \exp\left(\frac{GSI-100}{28-14D}\right) \\ s = exp\left(\frac{GSI-100}{9-3D}\right) \end{cases} \tag{45}$$

Where $m_i$ stands for strength constant for geomaterials; $D$ represents a parameter related to the degree of rock mass perturbation. Broadly speaking, $D \in [0, 1]$ where 0 traduces undisturbed rock mass, and 1 wholly disturbed rock mass.

The strain and displacement are correlated. In the visco-elastic zone, this correlation can be given as below:

$$\begin{cases} \varepsilon_\theta = \frac{u}{r} \\ \varepsilon_r = \frac{du}{dr} \end{cases} \tag{46}$$

Also, we can write:

$$\begin{cases} \sigma_1 = \sigma_\theta \\ \sigma_3 = \sigma_r \end{cases} \tag{47}$$

By replacing Equation (42) into Equation (22) and by overlooking the viscoplastic part, and by taking into consideration Equations (46) and (47), the viscoelastic deformation of the host rocks can written as:

$$u_r^{ve} = \frac{2R_0^2 N_1 e^{2M}}{3G_1 r} + \frac{2R_0^2 N_1 e^{2M}}{3G_2 r}\left[1 - exp\left(-\frac{G_2}{\eta_2 \alpha} t^\alpha\right)\right] \tag{48}$$

Here $u_r^{ve}$ represents the creep deformation of the viscoelastic zone.

Preprints (www.preprints.org) | NOT PEER-REVIEWED | Posted: 6 September 2023 doi:10.20944/preprints202309.0359.v1



Concerning the visco-plastic zones of the tunnel, a non-associated plastic flow law is considered since the dilation undoubtedly occurs in the plastic zone. As stated by Manh et al. [46], viscoplastic strains and displacements can be therefore linked as below:

$$\frac{du_r^{vp}}{dr} + k_\phi \frac{u_r^{vp}}{r} = \varepsilon_r + k_\phi \varepsilon_\theta \tag{49}$$

Here the visco-plastic deformation of the surrounding rocks of tunnel is noted by $u_r^{vp}$; $\varepsilon_r$ is radial strain; $\varepsilon_\theta$ is hoop strain; the coefficient of dilation is indicated by $k_\phi$, and can be given as follows:

$$k_\phi = \frac{1+sin\phi}{1-sin\phi} \tag{50}$$

Adequate combination of Equations (22), (43), (47) and (49) leads to the following:

$$\frac{du_r^{vp}}{dr} + k_\phi \frac{u_r^{vp}}{r} = \left[\frac{1}{3G_1} + \frac{1}{G_p} + \frac{1}{3G_2}\left(1 - exp\left(-\frac{G_2}{\eta_2 \alpha} t^\alpha\right)\right) + k\left(\frac{t}{\eta_3}\right)^n (1-D)^{(1-n)}\right]\left(S_r^p + k_\phi S_\theta^p\right) - \left(1+k_\phi\right)\frac{S_s}{G_p} \tag{51}$$

The three-dimensional forms of $\sigma_r^p$ and $\sigma_\theta^p$ which are respectively $S_r^p$ and $S_\theta^p$ can be written as follows:

$$\begin{cases} S_r^p = -\frac{(3+sin\varphi)}{12} m\sigma_c ln\frac{r}{R_0} - \frac{(3+sin\varphi)}{6}\sigma_c\sqrt{s} \\ S_\theta^p = \frac{(3-sin\varphi)}{12} m\sigma_c ln\frac{r}{R_0} + \frac{(3-sin\varphi)}{6}\sigma_c\sqrt{s} \end{cases} \tag{52}$$

From Equation (51), a function $g(t)$ can be defined as below:

$$g(t) = \left[\frac{1}{3G_1} + \frac{1}{G_p} + \frac{1}{3G_2}\left(1 - exp\left(-\frac{G_2}{\eta_2 \alpha} t^\alpha\right)\right) + k\left(\frac{t}{\eta_3}\right)^n (1-D)^{(1-n)}\right] \tag{53}$$

There is compatibility of deformations at the existing interface between the visco-plastic and visco-elastic zones. This condition is taken into account to evaluate the global visco-plastic deformation of the host rocks. At the aforesaid interface, this condition can be written as follows:

$$\begin{cases} r = R_P \\ u_r^{vp}(R_P, t) = u_r^{ve}(R_P, t) \end{cases} \tag{54}$$

Subsequently, we can have the following:

$$u_r^{vp}(R_P, t) = u_r^{ve}(R_P, t) = \frac{2R_0^2 N_1 e^{2M}}{3G_1 R_P} + \frac{2R_0^2 N_1 e^{2M}}{3G_2 R_P}\left[1 - exp\left(-\frac{G_2}{\eta_2 \alpha} t^\alpha\right)\right] \tag{55}$$

The global visco-plastic deformation of the surrounding rocks (dry states) of the tunnel is assessed by combining Equations (51) to (55). Its expression is given by:

$$\begin{aligned} u_r^{vp}(t) = {} & \frac{m\sigma_c}{12} g(t)\left[k_\phi(3-sin\phi) - (3+sin\phi)\right] g_1(r) + \frac{\sigma_c\sqrt{s}}{6} g(t)\left[k_\phi(3-sin\phi) - (3+sin\phi)\right] g_2(r) + \left(1+k_\phi\right)\frac{S_s}{G_p} g_2(r) \\ & + \frac{2R_0^2 N_1 e^{2M}}{3G_1 R_P} + \frac{2R_0^2 N_1 e^{2M}}{3G_2 R_P}\left[1 - exp\left(-\frac{G_2}{\eta_2 \alpha} t^\alpha\right)\right] g_3(r) \end{aligned} \tag{56}$$

The sub-functions $g_1(r)$, $g_2(r)$, and $g_3(r)$ are defined as follows:

$$\begin{cases} g_1(r) = \frac{r}{k_\phi+1}\left(ln\frac{r}{R_0}\right) - \frac{R_P}{k_\phi+1}\left(\frac{R_P}{r}\right)^{k_\phi}\left(ln\frac{R_P}{R_0}\right) - \frac{\left(r - R_P\left(\frac{R_P}{r}\right)^{k_\phi}\right)}{\left(1+k_\phi\right)^2} \\ g_2(r) = \frac{\left(r - R_P\left(\frac{R_P}{r}\right)^{k_\phi}\right)}{1+k_\phi} \\ g_3(r) = \left(\frac{R_P}{r}\right)^{k_\phi} \end{cases} \tag{57}$$

For the second variant which takes into account the effects of the pore water pressure, closed-form solutions are also conceived. Following the same steps as above, the global viscoplastic deformation of the tunnel, under the influence of pore water pressure, can be computed as:

Preprints (www.preprints.org) | NOT PEER-REVIEWED | Posted: 6 September 2023 doi:10.20944/preprints202309.0359.v1



$$u_r^{vp}(t,\sigma,p) = \frac{m\sigma_c}{12}h(t)\left[k_\phi(3-sin\phi)-(3+sin\phi)\right]g_1(r) + \frac{\sigma_c\sqrt{s}}{6}g(t)\left[k_\phi(3-sin\phi)-(3+sin\phi)\right]g_2(r) + \left(1+k_\phi\right)\frac{S_s}{G_p}g_2(r) + \frac{2R_0^2N_1e^{2M}}{3G_1R_P} + \frac{2R_0^2N_1e^{2M}}{3G_2R_P}\left[1-exp\left(-\frac{G_2}{\eta_2\alpha}t^\alpha\right)\right]g_3(r) \quad (58)$$

The influence of pore water pressure is taken into consideration by the function $h(t)$ which is defined as follows:

$$h(t) = \frac{1}{2G_1\ (\sigma,\ p)} + \frac{1}{G_p\ (\sigma,\ p)} + \frac{1}{2G_2\ (\sigma,\ p)}\left[1-exp\left(-\frac{G_2\ (\sigma,p)}{\eta_2\ (\sigma,\ p)\alpha}t^\alpha\right)\right] + k\left(\frac{t}{\eta_3\ (\sigma,p)}\right)^n\left(e^{-\beta\ (\sigma,\ p)t}\right)^{(1-n)} \quad (59)$$

The sub-functions $g_1(r)$, $g_2(r)$, and $g_3(r)$ are previously defined in Equation (57).

*4.1. Sensibility Analysis*

The relevant parameters are adequately examined in order to validate the proposed clos-form solutions. Parameters such as $m_b, s$, and $k_\phi$ are calculated using Equations (44) and (45). Other parameters characterising the surrounding rocks of the tunnel are shown in Table 8.

**Table 8.** Parameter characteristics of the surrounding rocks.

| GSI values | $P_0$ (MPa) | $\sigma_c$ (MPa) | $\sigma_s$ (MPa) | $\phi$ (°) | $S$ | $m_b$ |
|---|---|---|---|---|---|---|
| 20 | 10 | 30 | 12 | 47 | 0 | 0.06 |
| 40 | 10 | 35 | 12 | 1.2 | 0.00035 | 0.804 |
| 60 | 10 | 35 | 12 | 2.8 | 0.0048 | 2.084 |

On the basis of GSI basic chart [47–49], the GSI values for argillaceous sandstone and sandstone are estimated. The GSI values of sandstone varies from 30 to 60; those of the argillaceous sandstone from 20 to 40. Note that the existing reality is put forward in order to evaluate the rock parameters [50–52]. In fact, GSI values are low for argillaceous sandstone; while those of pure sandstone are somewhat appreciable. Thereby, different values of GSI are employed for thorough sensibility analysis. Note that the sensibility analysis is carried out considering mainly the creep parameters of the surrounding rocks.

Results are presented in Figures 17 to 21. They mainly describe the time-dependent deformation of the tunnel. Specifically, instant elastic creep deformation, primary creep deformation, and steady creep deformation are displayed in these figures. Initially, owing to the quick effects of rock excavation, the tunnel deformation increases quickly, and this corresponds to the instant elastic deformation. The latter is followed by the primary creep deformation where there is decreasing rate in the deformation evolution. Subsequently, the secondary creep deformation is happened at a constant rate.

Creep parameters have significant influence on the evolution of creep deformation. When these parameters (for instance $G_1, G_2, G_p, \eta_3$) decrease, there is increased time-dependent deformation of the tunnel. This conforms well to the real situation. Thereby, Figures 17 to 20 give the long-term trend in the creep deformation of the host rocks.

Preprints (www.preprints.org) | NOT PEER-REVIEWED | Posted: 6 September 2023 doi:10.20944/preprints202309.0359.v1



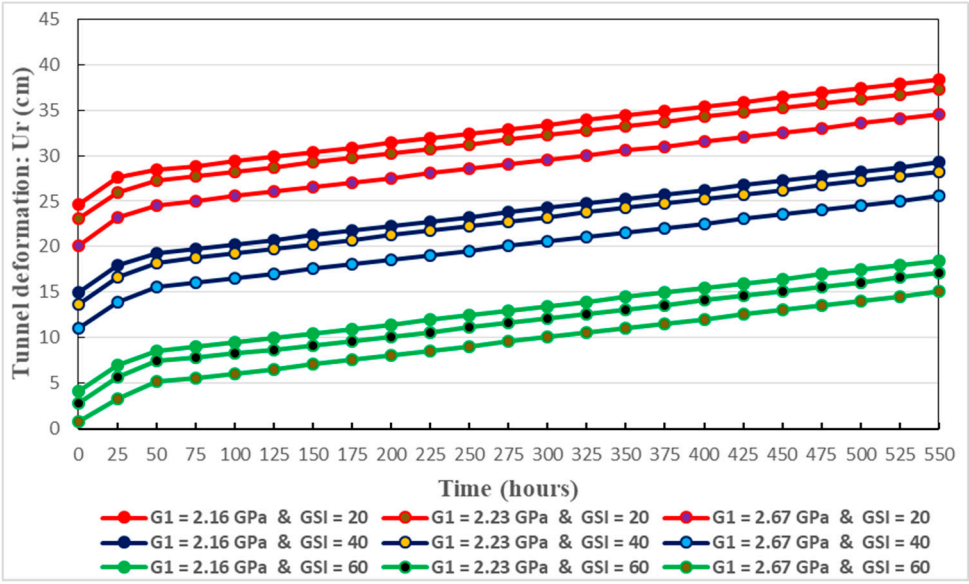


**Figure 17.** Time-dependent deformation of the tunnel considering different values of $G_1$ and GSI.

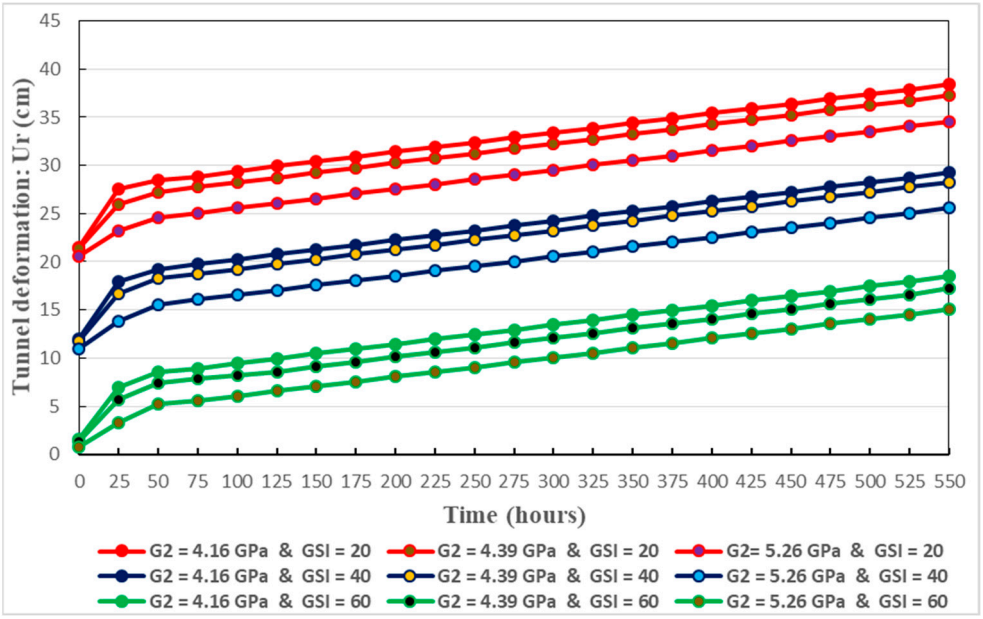


**Figure 18.** Time-dependent deformation of the tunnel considering different values of $G_2$ and GSI.

Preprints (www.preprints.org) | NOT PEER-REVIEWED | Posted: 6 September 2023 doi:10.20944/preprints202309.0359.v1



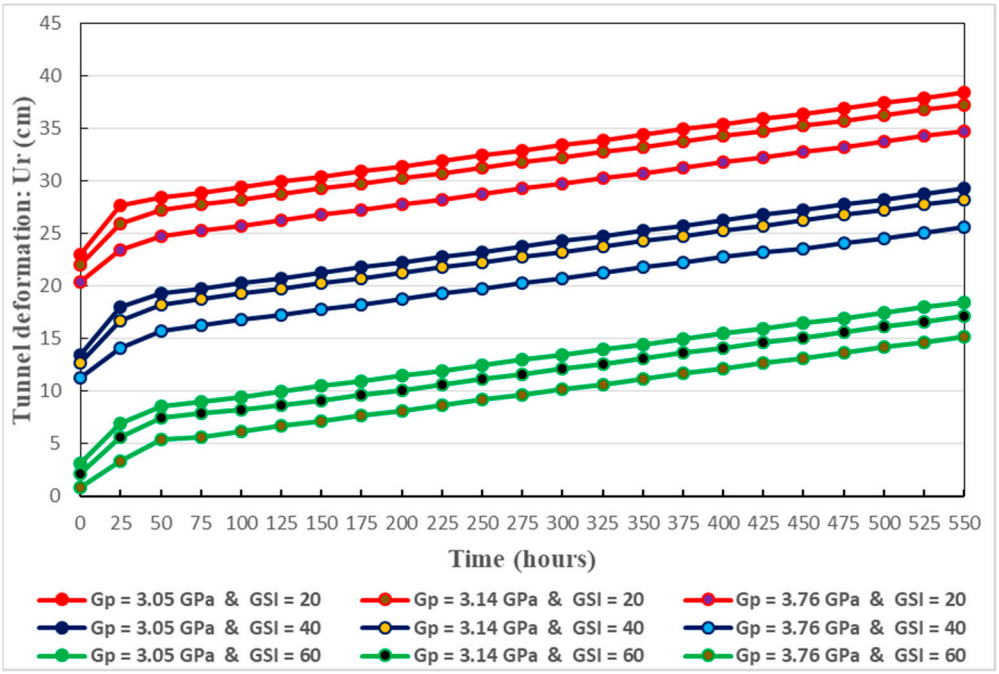


**Figure 19.** Time-dependent deformation of the tunnel considering different values of $G_p$ and GSI.

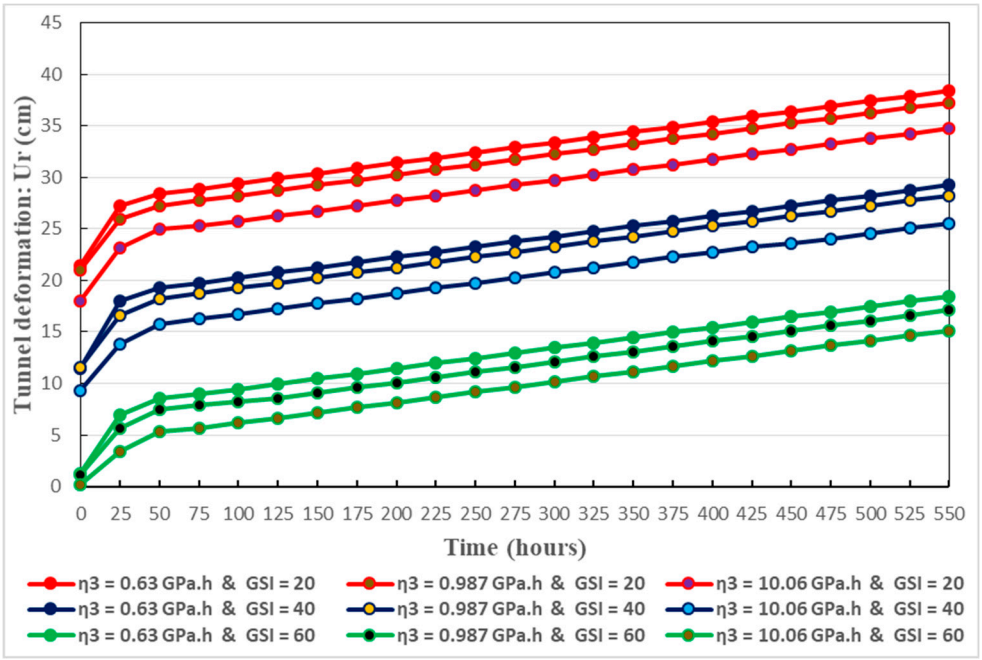


**Figure 20.** Time-dependent deformation of the tunnel considering different values of $\eta_3$ and GSI.

The relation between the tunnel wall deformation and the depth of the plastic zones is also studied. Figures 21 to 24 illustrate this relation. They reveal that, the deformation of the surrounding rock diminishes as the distance from the tunnel wall augments. Initially, the decrease in the deformation of the host rocks is rapid. Afterwards, the deformation keep decreasing at constant rate. Consequently, no matter the GSI values, the maximum creep deformation can be found at the tunnel wall, in accordance with the actual situation. It should be noted that, the tunnel deformation increases according to the tendencies of the plastic radius. More specifically, the increase of tunnel wall deformation is mainly caused by the increase in the depth of the plastic zone. It can be easily observed that the magnitudes of the plastic radii correspond to the extent of GSI values. Based on Figures 21

Preprints (www.preprints.org) | NOT PEER-REVIEWED | Posted: 6 September 2023 doi:10.20944/preprints202309.0359.v1



to 24, the radii of the tunnel's plastic zone for different creep parameters at three GSI values are shown in Table 9.

**Table 9.** Approximated values of the plastic zone radius for three GSI values.

| **GSI values** | 20 | 40 | 60 |
|---|---|---|---|
| **Radius of the plastic zone (m)** | 18 | 12 | 9 |

The strongest tunnel deformations are associated with the greatest plastic radii which are mainly generated by the lowest GSI values. Thereby, the large deformations of deep-buried tunnel are inevitable when soft rocks are initially weakened with poor mechanical properties. Mitigating tunnel wall deformations is of primary importance to limit the development of rock creep and guarantee the long-term safety and stability. Accurately forecasting the radius of the aforesaid zones should be counted as a mandatory task to adopt appropriate measures aiming at effectively limiting the deformation of deep soft rock tunnels.

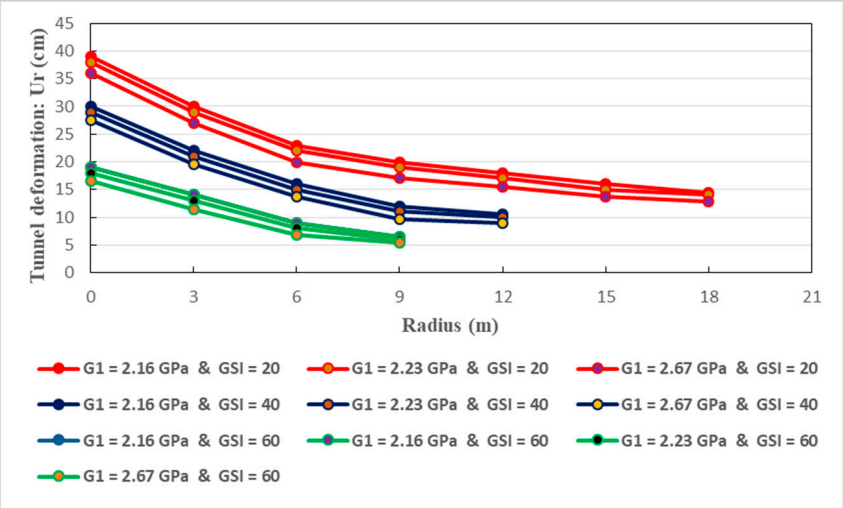


**Figure 21.** Visco-deformation of the tunnel host rocks with depth considering $G_1$.

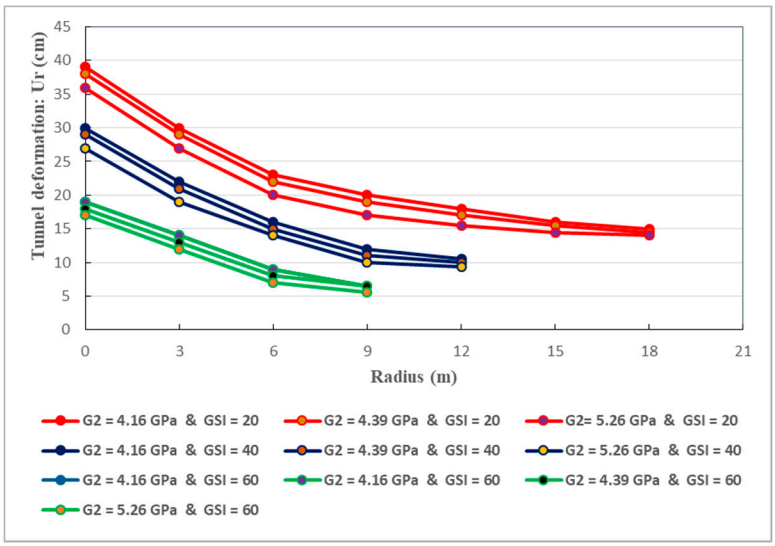


**Figure 22.** Visco-deformation of the tunnel host rocks with depth considering $G_2$.

Preprints (www.preprints.org) | NOT PEER-REVIEWED | Posted: 6 September 2023 doi:10.20944/preprints202309.0359.v1



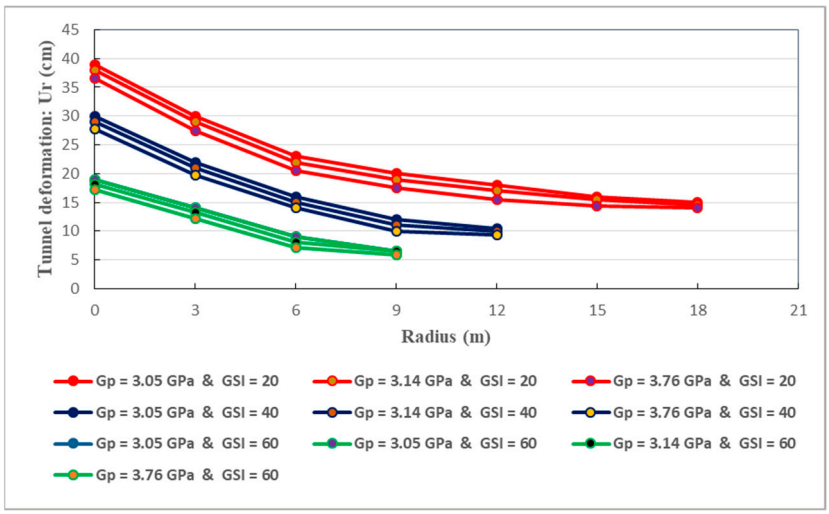


**Figure 23.** Visco-deformation of the tunnel host rocks with depth considering $G_p$.

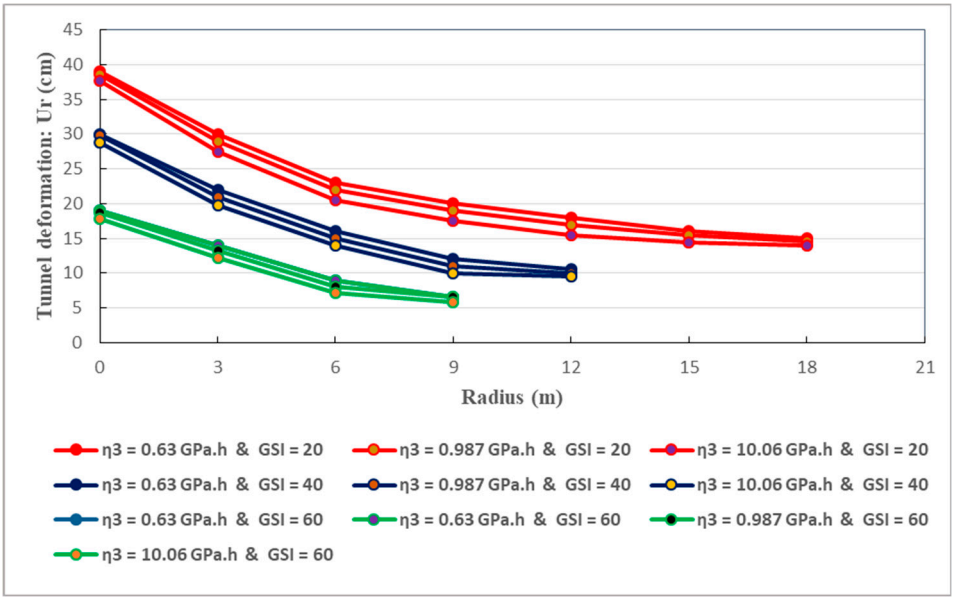


**Figure 24.** Visco-deformation of the tunnel host rocks with depth considering $\eta_3$.

*4.2. Assessment of Convergence Deformation in the Weilai Tunnel*

Forecasting the convergence deformation of the any deep-buried tunnels is of particular importance in ensuring their long-term stability. It is even more indispensable when the geological and hydrological conditions of the surrounding rocks are unfavorable. In fact, the convergence deformation is a key factor related to the safety and stability of deep tunnels. To evaluate the convergence deformation of the Weilai tunnel, the proposed closed-form solutions are utilized, and the results are compared with the on-site monitoring data. Total station and convergence gauges are conventionally used in the monitoring of critical points (roof and sidewalls) in the tunnel. One considers 27 days monitoring data. The size of the tunnel cross-section and the monitoring disposition points are illustrated in Figure 25.

Preprints (www.preprints.org) | NOT PEER-REVIEWED | Posted: 6 September 2023 doi:10.20944/preprints202309.0359.v1



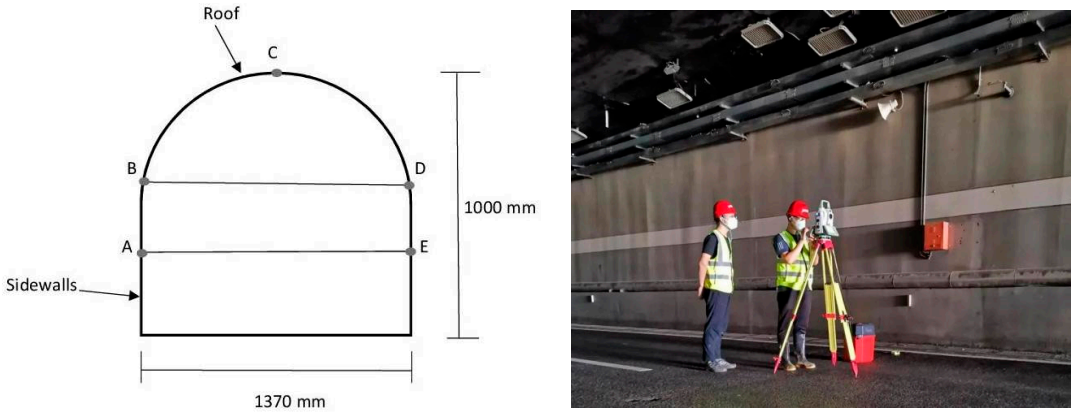


**Figure 25.** Illustration of tunnel cross-sectional size and arrangement of monitoring points.

From the cross-sectional area (S) of the tunnel, the equivalent radius ($R_e$) of the tunnel is calculated as below [44]:

$$R_e = \sqrt{\frac{S}{\pi}} \tag{60}$$

Using the two variants of the closed-form solutions, the convergence deformations of the tunnel are evaluated and are compared to the on-site monitoring data. In Figure 26, the results are presented.

Figure 26 clearly shows that good agreements are found between the calculated convergence deformation and the on-site monitoring data. It can be observed that, the convergence deformation in the tunnel roof is very close to the new model. Although they have lower numerical values, the sidewall convergences (A-E) and (B-D), in terms of behavior, are also close to the new model. The proposed closed-form solutions can therefore well forecast the time-dependent deformation of the Weilai tunnel.

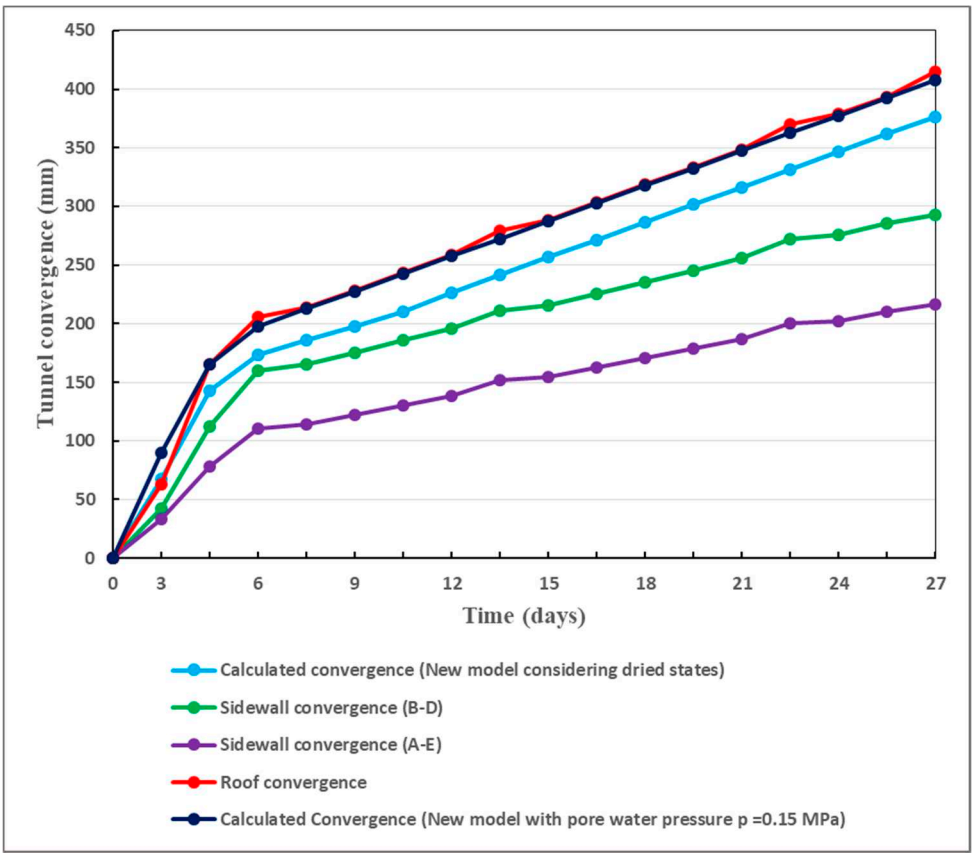


**Figure 26.** Calculated convergence deformation compared with on-site monitoring data.

 doi:10.20944/preprints202309.0359.v1



## 5. Relevant Measures Guaranteeing the Tunnel Long-Term Stability

Since the convergence deformation is large and the rocky environment of the tunnel is complex, the requirements for the supporting structure are considerable. In such conditions, stresses in the supporting structure will be very strong [53]. An adequate and robust support scheme is required to properly ensure the long-term stability of the tunnel. In spite of that, it should be recognized that the long-lasting performance of the support structure will be incontestably attacked by fatigue and ageing. This relates to all components of any given deep rock tunnel support system. For instance, the durability of typical primary support (rock bolts, cable bolts) can be diminished under the actions of major factors including rock creep [54]. Besides, excessive deformation of soft rock tunnels can even seriously jeopardize the secondary support [55]. Mostly, as pointed out by Galler and Lorenz [56], the widely employed materials for the tunnel secondary support are reinforced concrete and steel plate. However, the long-term performance of these materials is affected by corrosion which is almost inevitable in deep underground structures. In fact, as a result of groundwater leaks, deterioration and deformations in concrete structures can be increasingly severe over time [57,58]. The deformation of the Weilai tunnel is considerably exceeded compared to the established limit, as shown in Table 10, where H is the height of the tunnel which is 1000 mm.

**Table 10.** Allowable relative displacement around the tunnel.

| Surrounding rock grade | Adopted relation of the limit relative displacement | Limit relative displacement (mm) |
|---|---|---|
| Class IV | 0.05H | 50 |
| Class V | 0.08H | 80 |

It should be noted that, over the whole length of the Weilai Tunnel, the surrounding rock grades IV and V represent respectively 48.18% and 53.62% (right line), and 43% and 56.12% (left line). Specific values of the convergence deformation can be read in Figure 26. The extent of exceeded displacements is presented in Table 11.

**Table 11.** Allowable relative displacement around the tunnel.

| Surrounding rock grade | Scope of exceeded displacements with regard to the limitation (mm) | | |
|---|---|---|---|
| | **Roof** | **Sidewall A-B** | **Sidewall D-E** |
| **Class IV** | 8.5 times | 6 times | 4.5 times |
| **Class V** | 5.3 times | 3.7 times | 2.8 times |

Based on the major factors affecting the performance and durability of the typical primary support [54], and related engineering practices, to ensure tunnel stability, a robust support system was offered. Concretely, the adopted scheme of the support structure is as follows: Pressure aid + Deep grouting + Rock bolts + Cable bolts + Steel arch + Secondary lining. Nonetheless, as explained above, it is necessary to adequately and durably monitor the structural components of the tunnel. To this end, appropriate remote sensors are strongly suggested to ensure acceptable structural integrity and safety at time times [59]. In harsh rock environments, traditional monitoring techniques cannot provide real-time alerts on the health status of deep soft rock tunnels. In this sense, it is of great significance to opt for reliable monitoring methods, as relayed by Farahani et al. [60] and Nsubuga et al. [61]. Indeed, the primary support and the secondary support must be properly monitored thanks to high-performance monitoring systems capable of providing effective information in real time on the state of health of the tunnel. Thus, long-term safety and stability can be effectively ensured by making reliable decisions within a reasonable period of time regarding the current situation of the tunnel.

## 6. Discussions

The long-term stability of deep-buried tunnels in soft rock stratum is comprehensively studied in this article. It is shown that large deformations are particularly inevitable in such tunnels and are affected by major factors such as high stress and pore water pressure. In this situation, the host rock mechanical properties are degenerated, and considerable instability and failure in these underground structures are common [62–64]. On top of that, although drill-and-blast excavation method causes extra damage to the host rocks [14,65], it is imposed under complex geological and hydrological conditions of rocky media. Accordingly, to effectively guarantee the long-term stability of deeply buried tunnels in complex soft rocks, high reliable measures must be adopted and prevent the triggering of the tertiary creep. In fact, the latter is associated with huge deformations of deep-buried tunnels in soft rocks [66]. In this sense, the two variants of the novel creep constitutive model are designed in order to address as accurately as possible the time-varying deformations of the rocks surrounding the Weilai tunnel. It is in the same order of ideas that the two closed-form solutions are proposed. Other variants could also be designed. For instance, as temperature variation also affects rock creep, a related variant could be conceived. However, it is very difficult to cover everything in this paper.

It should be highlighted that, although the proposed creep constitutive model has the advantages of accurately capturing the comportment of deep soft rocks, it has two main drawbacks. On the one hand, it contains at least 9 parameters whose evaluation for loading and unloading processes takes considerable time. On the other hand, triaxial creep tests performed under load-unload cycles are necessary for precise model applications. It should be noted that the second variant of the creep model and that of the closed-form solution better describe the conditions of the studied deep soft rock tunnel. The designed closed-form solutions are utilized to evaluate the convergence deformation in terms of creep deformations of the deep soft rock tunnel. It is shown that the tunnel exhibits large creep deformations which surpasses 400 mm after only 27 days of excavation. This shows that, after excavation, the tunnel deformation increases quickly, owing to the complexity related to the regional environment (poor rock mass quality, high stress, presence of groundwater). To limit the creep deformation in this tunnel, quick installation of a suitable and robust support strongly imposed. Despite that, to effectively ensure the long-term safety and stability of the deep-buried tunnel in soft rocks, long-term monitoring of its structure is required. In fact, not only tunnels can be considered as risky structures [67], some uncertainties during their design and construction should be recognized [68]. Thereby, continuous monitoring of the tunnel structural health is promising. Since traditional monitoring techniques cannot provide regularly the actual tunnel health conditions [69], appropriate remote sensors are necessary to ensure the reliable operation of the tunnel at all times. Normally, each structural component of the tunnel should be adequately monitored.

## 7. Conclusions

To study the time-dependent deformation of deep-buried tunnels in soft rocks, the host rocks of the Weilai Tunnel in China's Guangxi province has been taken as the main research substance. A novel visco-elasto-plastic creep constitutive model with two variants are designed. Moreover, two closed form solutions are proposed to properly forecast the convergence deformation of the tunnel. The main conclusions drawn from this paper are as follows:

1. Typical load-unload cycles of rock excavation are employed to design the novel creep constitutive model. Major factors such as damage and the time-to-failure are accounted in the first variant of the proposed creep model, and additionally to these, pore water pressure is considered in the second variant of the model. Suitable experimental data are employed to validate the creep constitutive model and good agreements are found.
2. The second variant of the proposed creep constitutive model shows that pore water pressure has enormous influence on the development of creep in soft rocks. It better captures the actual relevant conditions of the deep-buried tunnels located in complex soft rock environments.

3. The conversion of the novel creep constitutive model into the two closed-form solutions is mainly based on the Hoek-Brown criterion. Comprehensive parametric investigations show that the geological strength index of the rocky media and creep parameters deeply influence the deformation comportment of deep-buried tunnels.
4. Comparisons between the calculated convergence deformations and the on-site monitoring data are adequately made, and good conformity is found. It is releveled that, in only 27 days, the Weilai tunnel suffers large convergence deformation which is greater than 400 mm. This deformation greatly exceeds the established deformation limit in the entire alignment of the tunnel. As suitable measures, robust support scheme and adequate long-term monitoring with appropriate remote sensors are strongly suggested to effectively ensure the long-term safety and stability of the studied tunnel.
5. To better describe the time-dependent behavior of deep soft rock tunnels, it is suggested to design creep constitutive model with variants. Comparisons between the behavior of the variants and the experimental or field data can provide clear indications on the analytical solutions which can really represent the time-varying deformations of deep soft rock tunnels.

**Author Contributions:** Conceptualization, W.F.; methodology, W.F.; software, W.F.; validation, HP; formal analysis, HP; investigation, W.F.; resources, W.F.; data curation, W.F; writing—original draft preparation, W.F; writing—review and editing, W.F; visualization, HP; supervision, H.P.; project administration, H.P.; funding acquisition, H.P. All authors have read and agreed to the published version of the manuscript.

**Funding:** This research was funded the Special Topics of National Key Research and Development Program of China, grant number 2022YFC3005603-01.

**Institutional Review Board Statement:** Not applicable

**Informed Consent Statement:** Not applicable

**Data Availability Statement:** Not applicable

**Conflicts of Interest:** The authors declare no conflict of interest.

## References

1. Brown, E.T., Bray, J.W., Ladanyi, B., Hoek, E. Ground Response Curves for Rock Tunnels. *J. Geotech. Eng.* **1983**, 109 (1), 15-39. https://doi.org/10.1061/(ASCE)0733-9410(1983)109:1(15)
2. Egger, P. Design and construction aspects of deep tunnels (with particular emphasis on strain softening rocks). *Tunn. Undergr. Space Technol.* **2000**, 15(4), 403-408. https://doi.org/10.1016/S0886-7798(01)00008-6.
3. Chin, P.H.; Rogers, J.D. Creep Parameters of Rocks on an Engineering Scale. *Rock Mech. Rock Eng.* **1987**, 20, 137–146. https://doi.org/10.1007/BF01410044
4. Tomanovic, Z. Rheological model of soft rock creep based on the tests on marl. *Mech Time-Depend. Mater.* **2006**, 10, 135–154. https://doi.org/10.1007/s11043-006-9005-2
5. Pietruszczak, S., Lydzba, D., Shao, J.F. Description of Creep in Inherently Anisotropic Frictional Materials. *J. Eng. Mech.* **2004**, 130(6), 681-690. https://doi.org/10.1061/(ASCE)0733-9399(2004)130:6(681)
6. Chen, W., Konietzky, H. Simulation of heterogeneity, creep, damage and lifetime for loaded brittle rocks. *Tectonophysics* **2014**, 633, 164–175. https://doi.org/10.1016/j.tecto.2014.06.033
7. Zhu, Y., Chen, L., Zhang, H., Zhou, Z., Chen, S. Physical and Mechanical Characteristics of Soft Rock Tunnel and the Effect of Excavation on Supporting Structure. *Appl. Sci.* **2019**, 9, 1517. DOI: https://doi.org/10.3390/app9081517
8. Yang, C., Jing, W., Daemen, J.J.K., Zhang, G., Du, C. Analysis of major risks associated with hydrocarbon storage caverns in bedded salt rock. *Reliability Eng. Syst. Safety* **2013**, 113, 94–111. https://doi.org/10.1016/j.ress.2012.12.017
9. Deng, H.S., Fu, H.L., Shi, Y., Zhao, Y.Y., Hou, W.Z. Countermeasures against large deformation of deep-buried soft rock tunnels in areas with high geostress: A case study. *Tunn. Undergr. Space Technol.* **2022**, 119, 104238. https://doi.org/10.1016/j.tust.2021.104238
10. Feng X. Experiment and Numerical Simulation on Creep Mechanical Behaviors of Mudstone under Unloading Condition. *Geofluids* **2022**, 2022, 7175774. https://doi.org/10.1155/2022/7175774
11. Quevedo, F.P.M., Bernaud, D., Filho, A.C. Numerical Analysis of Deep Tunnels in Viscoplastic Rock Mass Considering the Creep and Shrinkage of the Concrete Lining. *Int. J. Geomech.* **2022**, 22(4), 04022005. https://doi.org/10.1061/(ASCE)GM.1943-5622.0002282

12. Xue, Y., Kong, F., Li, S., Qiu, D., Su, M., Li, Z., Zhou, B. Water and mud inrush hazard in underground engineering: genesis, evolution and prevention. *Tunn. Undergr. Space Technol*. **2021**, 114, 103987. https://doi.org/10.1016/j.tust.2021.103987
13. Peng, H., Frenelus, W., Zhang, J. Key factors influencing analytical solutions for predicting groundwater inflows in rock tunnels. *Water Supply* **2022**, 22 (11), 7982-8013. https://doi.org/10.2166/ws.2022.369
14. Frenelus, W., Peng, H., Zhang, J. Long-term degradation, damage and fracture in deep rock tunnels: A review on the effect of excavation methods. *Fratt. Ed Integrità Strutt*. **2021**, 15(58), 128-150. https://doi.org/10.3221/IGF-ESIS.58.10
15. Torbica, S., Lapčević, V. Rock fracturing mechanisms by blasting. *Undergr Min. Eng*. **2018**, 32, 15-31. https://10.5937/PodRad1832015T
16. Li, X.B., Chen, Z.H., Weng, L., Li, C.J. Unloading responses of pre-flawed rock specimens under different unloading rates. *Transat. Nonferrous Met. Soc. China* **2019**, 29: 1516−1526. https://doi.org/10.1016/S1003-6326(19)65059-4
17. Fan, Y., Zheng, J.W., Cui, X.Z., Leng, Z.D., Wang, F., Lv, C.C. Damage zones induced by in situ stress unloading during excavation of diversion tunnels for the Jinping II hydropower project. *Bull. Eng. Geol. Environ*. **2021**, 80: 4689-4715. https://doi.org/10.1007/s10064-021-02172-y
18. Zheng, H., Cai, Q., Zhou, W., Lu, X., Li, M., Qi, C., Jiskani, I.M., Zhang, Y. Creep Behaviours of Argillaceous Sandstone: An Experimental and Modelling Study. *Appl. Sci*. **2020**, 10, 7602. https://doi.org/10.3390/app10217602
19. Shahbazi A, Saeidi A, Chesnaux R. A review of existing methods used to evaluate the hydraulic conductivity of a fractured rock mass. *Eng. Geol.* **2020**, 265, 105438. https://doi.org/10.1016/j.enggeo.2019.105438
20. Shu, S., Yao, Z., Xu, Y., Wang, C., Hu, K. Mechanical Properties and Constitutive Relationship of Cretaceous Frozen Sandstone under Low Temperature. *Appl. Sci*. **2023**, 13:4504. https://doi.org/10.3390/app13074504
21. Stille, H, Palmström, A. Ground behaviour and rock mass composition in underground excavations. *Tunn. Undergr. Space Technol*. **2008**, 23 (1): 46–64. https://doi.org/10.1016/j.tust.2006.11.005
22. Frenelus, W., Peng, H., Zhang, J. Evaluation methods for groundwater inflows into rock tunnels: a state-of-the-art review. *Int. J. Hydro*. **2021**, 5(4), 152–168. https://doi.org/10.15406/ijh.2021.05.00277
23. Zhao, B., Li, Y., Huang, W., Yang, J., Sun, J., Li, W., Zhang, L., Zhang, L. Mechanical characteristics of red sandstone under cyclic wetting and drying. *Environ. Earth Sci*. **2021**, 80, 738. https://doi.org/10.1007/s12665-021-10067-0
24. Birchall, T.J., Osman, A.S. Response of a tunnel deeply embedded in a viscoelastic medium. *Int. J. Numer. Anal. Meth. Geomech*. **2012**, 36, 1717–1740. https://doi.org/10.1002/nag.1069
25. Frenelus, W., Peng, H., Zhang, J. Creep Behavior of Rocks and Its Application to the Long-Term Stability of Deep Rock Tunnels. *Appl. Sci.* **2022**, 12(17), 8451; https://doi.org/10.3390/app12178451
26. Ma, C., Zhan, H.B., Yao, W.M., Li, H.Z. A new shear rheological model for a soft interlayer with varying water content. *Water Sci. Eng*. **2018**, 11(2), 131-138. https://doi.org/10.1016/j.wse.2018.07.003
27. Yang SD, Tan WJ, Fang YX. Study on creep mechanical properties and long-term strength of quartz sandstone. *Water Power* **2021**, 47(04), 43–50.
28. Liu, E.L., He, S.M. Effects of cyclic dynamic loading on the mechanical properties of intact rock samples under confining pressure conditions. *Eng. Geol., 2012*, 125(27), 81–91. https://doi.org/10.1016/j.enggeo.2011.11.007
29. Yang, S.Q., Hu, B. Creep and long-term permeability of a red sandstone subjected to cyclic loading after thermal treatments. *Rock Mech. Rock Eng. 2018*, 51, 2981–3004. https://doi.org/10.1007/s00603-018-1528-8
30. Liu, C., Yu, B., Zhang, D., Zhao, H. Experimental study on strain behavior and permeability evolution of sandstone under constant amplitude cyclic loading-unloading. *Energy Sci. Eng*. **2020**, 8, 452–465. https://doi.org/10.1002/ese3.527
31. Zhao, Y., Zhang, L., Wang, W., Wan, W., Li, S., Ma, W., Wang, Y. Creep Behavior of Intact and Cracked Limestone Under Multi-Level Loading and Unloading Cycles. *Rock Mech. Rock Eng. 2017*, 50, 1409–1424. https://doi.org/10.1007/s00603-017-1187-1
32. Sterpi, D., Gioda, G. Visco-plastic behaviour around advancing tunnels in squeezing rock. *Rock Mech. Rock Eng*. **2009**, 42, 319–339. https://doi.org/10.1007/s00603-007-0137-8
33. Deng, P., Liu, Q., Ma, H., He, F., Liu, Q. Time-dependent crack development processes around underground excavations. *Tunn. Undergr. Space Technol*. **2020**, 103, 103518. https://doi.org/10.1016/j.tust.2020.103518
34. Deng, H.F., Zhou, M.L., Li, J.L., Sun, X.S., Huang, Y.L. Creep degradation mechanism by water-rock interaction in the red-layer soft rock. *Arab. J. Geosci*. **2016**, 9, 601. https://doi.org/10.1007/s12517-016-2604-6
35. Jaeger, J.C., Cook, N.G., Zimmerman, R. Fundamentals of rock mechanics. John Wiley & Sons, **2009**.
36. Ramberg, W., Osgood, W.R. Description of stress–strain curves by three parameters, in: Technical Note (902). National Advisory Committee for Aeronautics, Washington DC, **1943**.

37. Kachanov, L.M. Rupture time under creep conditions. *Int. J. Fract.* **1999**, 97, 11–18. https://doi.org/10.1023/A:1018671022008
38. Kachanov, L.M. Effective elastic properties of cracked solids: critical review of some basic concepts. *Appl. Mech. Reviews*, **1992**, 45 (8), 304–335. https://doi.org/10.1115/1.3119761
39. Marquardt, D.W. An algorithm for least-squares estimation of non-linear parameters. *J. Soc. Industr. Appl. Math*. **1963**, 11 (2), 431-441. https://doi.org/10.1137/0111030
40. Jiang, H., Sun, H., Shi, K., Xu, J. Stability Analysis of the Surrounding Rock-Lining Structure in Deep-Buried Hydraulic Tunnels Having Seepage Effect. *Sustainability* **2022**, 14, 16586. https://doi.org/10.3390/su142416586
41. Li, G., Liang, B. Experimental research on the effect of pore water pressure on the creep laws of soft rock. *J. China Coal Soc*. **2009**, 34(8), 1067-1070.
42. Peng, K., Yi, G., Luo, S., Si, X. Stress Analysis and Spalling Failure Simulation on Surrounding Rock of Deep Arch Tunnel. *Appl. Sci.* **2023**, 13, 6474. https://doi.org/10.3390/app13116474
43. Hoek, E, Brown, E.T. The Hoek – Brown failure criterion and GSI – 2018 edition. *J. Rock Mech. Geotech. Eng*. **2019**, 11, 445-463. https://doi.org/10.1016/j.jrmge.2018.08.001
44. Zhang, J.Z., Zhou, X.P., Yin, P. Visco-plastic deformation analysis of rock tunnels based on fractional derivatives. *Tunn. Undergr. Space Technol.* **2019**, 85, 209–219. https://doi.org/10.1016/j.tust.2018.12.019
45. Li, S., Ling, T., Liu, D., Liang, S., Zhang, R., Huang, B., Liu, K. Determination of Rock Mass Parameters for the RHT Model Based on the Hoek–Brown Criterion. *Rock Mech. Rock Eng*. **2023**, 56, 2861–2877. https://doi.org/10.1007/s00603-022-03189-9
46. Manh, H.T., Sulem, J., Subrin, D., Billaux, D. Anisotropic time-dependent modelling of tunnel excavation in squeezing ground. *Rock Mech. Rock Eng*. **2015**, 48 (6), 2301–2317. https://doi.org/10.1007/s00603-015-0717-y
47. Tsiambaos, G., Saroglou, H. Excavatability assessment of rock masses using the Geological Strength Index (GSI). *Bull. Eng. Geol. Environ*. **2010**, 69, 13–27. https://doi.org/10.1007/s10064-009-0235-9
48. Marinos, V., Carter, T.G. Maintaining geological reality in application of GSI for design of engineering structures in rock. *Eng. Geol*. **2018**, 239, 282–297. https://doi.org/10.1016/j.enggeo.2018.03.022
49. Song, Y., Xue, H., Ju, G. Comparison of different approaches and development of improved formulas for estimating GSI. *Bull. Eng. Geol. Environ*. **2020**, 79, 3105–3119. https://doi.org/10.1007/s10064-020-01739-5
50. Cai, M., Kaiser, P.K., Tasaka, Y., Minami, M. Determination of residual strength parameters of jointed rock masses using the GSI system. *Int. J. Rock Mech. Min. Sci.* **2007**, 44, 247–265. https://doi.org/10.1016/j.ijrmms.2006.07.005
51. Senent, S., Mollon, G., Jimenez, R. Tunnel face stability in heavily fractured rockmasses that follow the Hoek–Brown failure criterion. *Int. J. Rock Mech. Min. Sci*. **2013**, 60, 440–451. https://doi.org/10.1016/j.ijrmms.2013.01.004
52. Alejano, L.R., Alonso, E. Considerations of the dilatancy angle in rocks and rock masses. *Int. J. Rock Mech. Min*. Sci. **2005**, 42, 481–507. https://doi.org/10.1016/j.ijrmms.2005.01.003
53. Barla, G. Contributions to the understanding of time dependent behaviour in deep tunnels. *Geomech & Tunn*. **2011**, 4, 255-264. https://doi.org/10.1002/geot.201100021
54. Frenelus, W., Peng, H., Zhang, J. An Insight from Rock Bolts and Potential Factors Influencing Their Durability and the Long-Term Stability of Deep Rock Tunnels. *Sustainability* **2022**, *14*, 10943. https://doi.org/10.3390/su141710943
55. Chen, D., Wang, L., Versaillot, P.D., Sun, C. Triaxial creep damage characteristics of sandstone under high crustal stress and its constitutive model for engineering application. *Deep Undergr. Sci. Eng*. **2023**, 1-12. https://doi.org/10.1002/dug2.12033
56. Galler, R., Lorenz, S. Support elements in conventional tunneling – Focus on long-term behavior. *Undergr. Space*, **2018**, 3, 277–287. https://doi.org/10.1016/j.undsp.2018.01.009
57. Gong, J., Lambert, M.F., Simpson, A.R., Zecchin, A.C. Detection of Localized Deterioration Distributed along Single Pipelines by Reconstructive MOC Analysis. *J. Hydraul. Eng*. **2014**, 140(2), 190-198. https://doi.org/10.1061/(ASCE)HY.1943-7900.000080
58. Zeng, W., Gong, J., Cook, P.R., Arkwright, J.W., Simpson, A.R., Cazzolato, B.S., Aaron, C. Zecchin, A.C., Lambert MF. Leak Detection for Pipelines Using In-Pipe Optical Fiber Pressure Sensors and a Paired-IRF Technique. *J. Hydraul. Eng*. **2020**, 146(10), 06020013. https://doi.org/10.1061/(ASCE)HY.1943-7900.0001812
59. Frenelus, W., Peng, H. Towards Long-Term Monitoring of the Structural Health of Deep Rock Tunnels with Remote Sensing Techniques. *Frat. Ed Integrità Strutt*. **2023**, 17 (66), 56-87.
60. Farahani, B.V., Barros, F., Sousa, P.J., Cacciari, P.P., Tavares, P.J., Futaic, M.M., Moreira, P. A coupled 3D laser scanning and digital image correlation system for geometry acquisition and deformation monitoring of a railway tunnel. *Tunn. Undergr. Space Technol*. **2019**, 91, 102995. https://doi.org/10.1016/j.tust.2019.102995
61. Nsubuga, S., Tsakiri, M., Georgiannou, V. A smart decision tool for the prediction of tunnel crown displacements. *Appl. Geomat*. **2021**, 13, S77–S91. https://doi.org/10.1007/s12518-020-00304-9

62. Huang, X., Liu, Q., Liu, B., Liu, X., Pan, Y., Liu, J. Experimental Study on the Dilatancy and Fracturing Behavior of Soft Rock Under Unloading Conditions. *Int. J. Civ. Eng*. **2017**, 15, 921–948. https://doi.org/10.1007/s40999-016-0144-9
63. Zeng, C., Zhou, Y., Xiao, Y., Zhou, X., Zhu, C., Xu, Y. Research on Soft Rock Damage Softening Model and Roadway Deformation and Failure Characteristics. *Materials* **2022**, 15, 5886. https://doi.org/10.3390/ma15175886
64. Chen, L., Wang, Z., Wang, W., Zhang, J. Study on the Deformation Mechanisms of the Surrounding Rock and Its Supporting Technology for Large Section Whole Coal Cavern Groups. *Processes* **2023**, 11, 891. https://doi.org/10.3390/pr11030891
65. Hedayat, A., Oreste, P., Spagnoli, G. Analysis of the effects of blast-induced damage zone with attenuating disturbance factor on the ground support interaction. *Geomech. & Geoeng*. **2021**, 16(4), 277-287. https://doi.org/10.1080/17486025.2019.1664777
66. Xu, J., Wen, H., Sun, C., Yang, C., Rui, G. Numerical Simulation of Non-Stationary Parameter Creep Large Deformation Mechanism of Deep Soft Rock Tunnel. *Appl. Sci*. **2022**, 12, 5311. https://doi.org/10.3390/app12115311
67. Zaid M, Sadique MR. The response of rock tunnel when subjected to blast loading: Finite element analysis. *Eng. Reports* **2021**, 3, e12293. https://doi.org/10.1002/eng2.12293
68. Ma, J., Pei, H., Zhu, H., Shi, B., Yin, J. A review of previous studies on the applications of fiber optic sensing technologies in geotechnical monitoring. *Rock Mech. Bull*. **2023**, 2 (1), 100021. https://doi.org/10.1016/j.rockmb.2022.100021
69. Yang, H., Xu, X. Structure monitoring and deformation analysis of tunnel structure. *Composite Struct*. **2021**, 276, 114565. https://doi.org/10.1016/j.compstruct.2021.114565